Single-cell RNA sequencing implicates venous endothelial cells as a source of VEGF-mediated neo-angiogenesis in neuroinflammation

S. Shahriar[1], M. Z. Price[2], C. R. Wayne[3], M. D. Glendinning[3], G. Prochilo[2], H. Stuhlman[4], S. Biswas[3*], V. Menon[3*] and D. Agalliu[1, 3, 5*]

Departments of [1]Pathology & Cell Biology, [2]Biological Sciences and [3]Neurology, Columbia University Irving Medical Center, New York, NY 10032, USA.

[4]Department of Cell and Developmental Biology, Weill Cornell Medical College, New York, NY 10065, USA.

*equal contribution senior authors

[5] Corresponding author: E-mail: da191@cumc.columbia.edu

Mailing address:

Columbia University Irving Medical Center

650 West 168th Street

Black Building Room 310

New York, NY 10032

Telephone: 212-305-0323

ORCID: 0000-0002-5375-4143

ABSTRACT

Histopathological studies of multiple sclerosis (MS), a demyelinating disease of the central nervous system (CNS), and its animal model experimental autoimmune encephalomyelitis (EAE) have found newly formed leaky vessels in demyelinated acute and chronic plaques, in addition to blood-brain barrier damage in existing vessels, that exacerbate disease pathology by increasing CNS infiltration of immune cells. However, which vessel subtypes and signaling pathways generate these aberrant vessels is poorly understood. Using single-cell RNA sequencing and *in vivo* validation, we find that transcriptome signatures of neo-angiogenesis arise in venous endothelial cells in both acute and chronic EAE, and correlate with upregulation in VEGF-A signaling. These neo-angiogenic markers are also increased in human MS lesions. Treatment with a VEGF-A blocking antibody ameliorates EAE pathology by reducing neo-angiogenic transcriptomic signatures *in vivo*, suggesting that VEGF-A drives angiogenesis from vein ECs in EAE. Our findings suggest novel therapies targeting the vasculature that could benefit chronic MS.

INTRODUCTION

Multiple sclerosis (MS) is a chronic, autoimmune, inflammatory demyelinating disease of the central nervous system (CNS), in which activated leukocytes invade the CNS to trigger neuroinflammation, demyelination, gliosis, and axonal damage and resection[1,2]. Inflammation of CNS endothelial cells (ECs) associated with focal breakdown of the blood-brain barrier (BBB) is prevalent in demyelinating MS plaques[3]. Abnormalities in BBB tight junctions precede the onset of clinical experimental autoimmune encephalomyelitis (EAE), the animal model for MS, by pathological[4-7], MRI[8], and *in vivo* two-photon imaging studies[9], correlate with clinical severity in both MS[10,11] and EAE[4,5], and persist throughout the disease to promote migration of leukocytes

45 across the BBB[12-15]. Recent studies have shown that MS-associated single nucleotide
46 polymorphisms are enriched in ECs compared to other CNS cells[16], consistent with a critical role
47 for the CNS endothelium in MS pathogenesis.

48 Angiogenesis is most active during CNS development in rodents and humans, and is absent
49 in the adult CNS[17]. Neo-angiogenesis (formation of abnormal new vessels) is a second CNS vessel
50 abnormality, in addition to BBB damage from existing vessels, surrounding acute and chronic MS
51 plaques[18,19]. Many blood vessels within MS/EAE lesions have an irregular morphology[20], and
52 express some markers of proliferation[21]. Vessel density is increased in demyelinating lesions
53 during both peak and relapsing EAE, as well as relapsing-remitting MS (RRMS) and secondary
54 progressive MS (SPMS)[22-26]. Most studies suggest that angiogenesis worsens MS/EAE
55 pathogenesis[18,19] since its blockade improves clinical scores and attenuates demyelination and
56 inflammation in EAE[26,27]. However, the timing and relation of neo-angiogenesis to EAE/MS
57 progression, and its molecular characterization, vascular origin and underlying signaling pathways
58 remain poorly understood.

59 Vascular endothelial growth factor (VEGF) is a key mediator of angiogenesis in normal
60 vascular development[28], and in pathologies such as cancers[29], ocular conditions[30] and
61 inflammatory diseases. VEGF-A expression is upregulated in acute and chronic MS plaques[20] and
62 EAE[26,27]. Serum VEGF-A levels are significantly higher in relapsing MS, compared to either
63 remitting MS patients, or healthy cases, and correlate with lesion length on MRI examination[20,31].
64 Bevacizumab (Avastin®) is a recombinant, humanized monoclonal antibody that inhibits VEGF-
65 A by blocking its binding to VEGF receptor 2 (VEGFR2)[32-34]. Administration of either
66 bevacizumab, or the monoclonal antibody B20.4-1-1 that binds both murine and human VEGF-
67 A[27], in mice prior to and during EAE induction improves clinical disease and attenuates both

demyelination and inflammation[26,27]. Since VEGF-A is known to suppress host immunity in the tumor microenvironment[35], it is unclear whether VEGF-A blockade ameliorates EAE outcomes by inhibiting angiogenesis, or by reducing immune cell activation and CNS infiltration.

In addition to VEGF-A signaling, the Wnt/β-catenin pathway is critical for both developmental angiogenesis and BBB formation and maintenance in the healthy CNS[36-40]. We have previously shown that the Wnt/β-catenin pathway is reactivated in CNS ECs during EAE and MS; its inhibition in CNS ECs in mice prior to EAE onset exacerbates disease outcomes, increases $CD4^+$ T cell infiltration into the CNS, and exacerbates demyelination by increasing expression of Vascular cell adhesion molecule-1 (Vcam1) and Caveolin-1, two proteins critical for lymphocyte attachment and migration across the BBB[9,41]. Whether activation of the Wnt/β-catenin signaling in EAE/MS promotes neo-angiogenesis together with VEGF-A remains unknown.

To address which vessel subtypes and signaling pathways drive neo-angiogenesis and characterize its molecular signatures in neuroinflammation, we performed single-cell RNA sequencing (scRNAseq), and subsequent *in vivo* validation in control, acute and chronic MOG_{35-55} EAE mice. We find that transcriptomic signatures of neo-angiogenesis arise in venous ECs in both acute and chronic EAE, and correlate with upregulation in VEGF-A, but not Wnt/β-catenin, signaling. These neo-angiogenic markers are also increased in human MS lesions. Treatment with the VEGF-A blocking antibody bevacizumab at the disease onset, ameliorates EAE clinical pathology by reducing neo-angiogenic transcriptomic signatures *in vivo*, without affecting activation and infiltration of immune cells into the CNS. Our study provides a comprehensive molecular understanding of the origin and mechanism of neo-angiogenesis in EAE/MS, and suggests novel therapies targeting the pathological vasculature that could benefit individuals with chronic MS.

RESULTS

ECs isolated from spinal cords of control and EAE mice cluster based on A-V zonation and disease state

To determine which vessel subtypes and signaling pathways drive neo-angiogenesis in EAE, we induced MOG_{35-55} EAE in 12-week-old *TCF/LEF1::*H2B::eGFP (Wnt reporter) female mice[9,41], and collected spinal cords at acute peak [score = 2-4; 16-17 days post-immunization (d.p.i.)] and early chronic (score ≤ 1; 28-29 d.p.i.) disease for scRNAseq (**Fig. 1a**). Age-matched healthy and Complete Freund's Adjuvant (CFA)-immunized mice served as controls. Acute and chronic EAE mice had a similar disease course with no difference in the day of disease onset or peak clinical score. The disease score on the day of collection was higher for the acute compared to chronic cohort (CFA mice did not have any disease; **Extended Data Fig. 1a-e**). Spinal cords were dissociated into single-cell suspensions and Wnt-positive ($eGFP^+$) and Wnt-negative ($eGFP^-$) $CD31^+$ ECs were sorted and combined for scRNAseq (**Extended Data Fig. 1f**). After quality filtering[42] and *in silico* EC selection based on expression of *Pecam1*, *Cldn5*, and *Erg*[43], we performed graph-based clustering to separate 45,309 ECs into distinct clusters based on their transcriptomic expression profiles.

Graph-based clustering separated the ECs into 23 distinct clusters, which were visualized using a *t*-distributed stochastic neighbor embedding (t-SNE) representation [**Fig. 1c-f**; batch correction was not required for clustering (**Extended Data Fig. 1j**)]. Within the vascular system, ECs lining the arteries, capillaries and veins have unique functions and transcriptional profiles (**Fig. 1b**); however, they undergo a gradual transcriptome change referred to as "zonation"[44]. We assigned a subtype identity to each EC cluster based on expression of canonical markers for each

vessel subtype (**Fig 1e, f; Extended Data Fig. 1g-i**). Expression of arterial and venous markers peaked at opposite ends of the t-SNE plot, separated by capillary clusters. Although non-local distances in t-SNE plots are highly nonlinear, the overall arrangement of cells suggests that arteriovenous (AV) zonation was a major axis of variation in the EC data (**Fig 1e**). The disease state was the second axis of variation since ECs purified from acute and chronic EAE formed separate groups from those isolated from controls (**Fig. 1c, d**). Since the proportions of arterial (aEC), capillary (cEC), venule (vnEC), and vein (vEC) ECs were similar among healthy and disease samples (**Extended Data Fig. 1k**), EC clustering was not driven by differences in vessel subtype representation. Hence, ECs undergo transcriptional shifts in both acute and chronic EAE as shown before by bulk and scRNAseq[45,46]. Quantification of *eGFP* mRNA expression within the single-cell dataset revealed that Wnt/β-catenin signaling was highest in cECs, moderate in aECs and vnECs, and low-to-absent in vECs (**Extended Data Fig. 1l**).

Transcriptomic signatures of neo-angiogenesis arise in venous ECs in both acute and chronic EAE

EC clusters belonging to each vascular subtype (6,856 aECs; 30,208 cECs; 6,596 vnECs, and 1,649 vECs) were grouped separately and visualized with t-SNE (**Fig. 2a-b, d-e, g-h, j-k**). Arterial ECs from acute EAE formed a separate sub-cluster from chronic EAE and control samples (these groups clustered together; **Fig. 2a-c**), indicating that transcriptomic changes induced by neuroinflammation are transient in aECs. In contrast, cECs, vnECs, and vECs isolated from control, acute, and chronic EAE formed distinct sub-clusters (**Fig. 2d-e, g-h, j-k**), indicative of more persistent transcriptomic changes during neuroinflammation. However, the control (healthy and CFA)-enriched cluster in both cEC and vnEC populations contain a higher proportion of ECs

originating from chronic than acute EAE (**Fig. 2f, i**). This implies that cECs and vnECs may start transitioning to a normal transcriptomic state as the disease enters a chronic phase. In contrast, the control-enriched cluster in vECs contains only a small percentage of ECs from chronic EAE (**Fig. 2l**). The control samples (healthy and CFA) have similar transcriptional profiles, except in vnECs where they cluster separately due to increased expression of inflammatory gene signatures in CFA (**Fig. 2g, h**; data not shown).

To identify key transcriptomic signatures differentiating ECs from distinct conditions, we performed differential gene expression (DE) analysis comparing either the acute- or chronic-EAE to control-enriched EC clusters for each vessel subtype (**Extended Data Table 1**). This data was used to conduct gene set enrichment analysis (GSEA) using curated and comprehensive gene catalogs for various cellular and molecular pathways and functions from the Molecular Signatures Database v6.1 (*MSigDB: software.broadinstitute.org/gsea/msigdb/genesets.jsp*) and published sources[47,48] and determine which processes were significantly up- and downregulated in diseased ECs from each vessel subtype (**Extended Data Table 1**).

Gene sets associated with inflammation, antigen processing and presentation, and chemokine/cytokine signaling were upregulated in all ECs from acute EAE (**Fig. 3a**), and those associated with inflammation and antigen processing and presentation were also upregulated in cECs and vECs from chronic EAE (**Fig. 3c**). In contrast, expression of the BBB gene set was significantly downregulated in diseased cECs, vnECs, and vECs in both acute and chronic EAE (**Fig. 3b, d**), consistent with a dysfunctional BBB[45,46]. Surprisingly, expression of BBB genes was upregulated in acute aECs relative to controls (**Fig. 3a**), which may explain the transient nature of neuroinflammatory transcriptomic changes in aECs (**Fig. 2b**).

Angiogenesis involves several steps ranging from tip and stalk EC specification, tip cell-mediated extracellular matrix (ECM) degradation, EC migration and proliferation[49]. Pathological tumor angiogenesis is also regulated, in part, by endothelial-to-mesenchymal transition (EndoMT), which induces delamination of resident ECs and subsequent acquisition of a mesenchymal phenotype with invasive/migratory properties[50,51]. DE analysis of diseased versus control vnECs and vECs revealed that the top-upregulated genes are angiogenic and tip cell markers in both acute and chronic EAE (**Fig. 3e**; **Extended Data Fig. 2**). Several angiogenesis ("tip cells", "angiogenesis", "EC proliferation" and "EC migration") and angiogenesis-related ("ECM" [52], "EndoMT" [53]) gene signatures are significantly upregulated in diseased veins (acute and chronic) together with two pro-angiogenic pathways ("VEGF" and "TGF-β")[54-56] (**Fig. 3a, c**). Acute vnECs also showed upregulation of gene signatures for tip cells in acute EAE (**Fig. 3a**). In contrast, arterial or capillary ECs in acute EAE were not enriched for transcriptional gene signatures of neo-angiogenesis compared to controls. In fact, expression of angiogenesis-related, and pro-angiogenic signaling gene sets were downregulated in diseased aECs relative to controls, suggesting a vascular repair process (**Fig. 3b**). Although several angiogenesis pathways were upregulated in EAE vECs, the Wnt/β-catenin signaling is almost absent in healthy vECs and downregulated in chronic EAE vECs (**Extended Data 1l; Fig. 3d**). In summary, our scRNAseq data reveal that transcriptomic signatures for neo-angiogenesis are upregulated in vECs, and to a lesser extent in vnECs, in acute and chronic EAE. While Wnt/β-catenin signaling is essential for developmental CNS angiogenesis[17], it is likely not associated with pathological neo-angiogenesis in EAE.

Congruency analysis reveals a unique transcriptome signature of neuroinflammation-related angiogenesis in EAE

We next asked to what extent neuroinflammation-related neo-angiogenesis shares similar transcriptomic signatures with either CNS developmental or tumor angiogenesis. We analyzed publicly available datasets of murine lung tumor ECs (TECs)[57] and developmental CNS ECs [DECs; embryonic day 14.5 (E14.5)][58] to establish a catalog of angiogenic genes that were significantly upregulated in expression during tumor and CNS developmental angiogenesis, respectively. Comparing those gene sets to the angiogenic gene signature of acute EAE vECs revealed that most angiogenic genes in neuroinflammation were also upregulated in developmental (~68%) and tumor (~85%) angiogenesis (**Extended Data Fig. 3a-b**). However, there was a greater number of acute EAE vEC genes shared with TECs than with DECs, suggesting that neuroinflammation angiogenesis is more similar at the molecular level with tumor, than developmental, angiogenesis. We also analyzed the congruency in angiogenic gene expression between DECs and TECs (**Extended Data Fig. 3c**). While pathogenic and developmental angiogenic gene signatures had some common genes (105), they also had a significant number of unique genes (DECs had 102 unique genes and TECs had 79), suggesting that the two processes are very different. Therefore, neuroinflammation and tumor angiogenesis have a higher congruency at the gene signature level, compared to neurodevelopmental angiogenesis.

To confirm these computational analyses *in vivo*, we analyzed expression of Apelin (*Apln*), one of the non-congruent angiogenic markers identified through the computational analysis between DECs and EAE vECs, in developing (P3), healthy adult, and acute EAE spinal cord tissues via RNA *in situ* hybridization (**Extended Data Fig. 3d-i**). *Apln* is a positive modulator of angiogenesis and is enriched in proliferating ECs and tip cells in the P7 brain[59]. *Apln*$^{-/-}$ mouse retinas show delayed EC proliferation, vascular outgrowth and branching[60]. Consistent with prior studies[59], we found that *Apln* mRNA is highly expressed by many developing blood vessels in the

P3 spinal cord; however, its expression is abolished in the healthy adult CNS, except in the vasculature of the choroid plexus and meninges, and in some neurons (**Extended Data Fig. 3d-i;** data not shown). *Apln* expression was not induced in the inflamed blood vessels located in white matter lesions of the spinal cord in acute EAE (**Extended Data Fig. 3d-i**), unlike other angiogenesis markers (see below), validating that neurodevelopmental and neuroinflammatory angiogenesis have distinct programs.

Venous ECs undergo proliferation and express angiogenesis markers in acute and chronic EAE

To validate our scRNAseq findings that vECs show transcriptomic features of angiogenesis in neuroinflammation (**Fig. 3**), we examined the expression of the proliferation marker Ki67 in arteries, capillaries, and veins in longitudinal (sagittal) spinal cord sections from control (CFA), acute and chronic EAE mice (**Fig. 4a**). A significantly higher proportion of Vcam1$^+$ vECs express Ki67 in both acute (~15%) and chronic (~11%) EAE, compared to the CFA control (~2%; **Fig. 4c-c'''**, **f**), consistent with scRNAseq data for the *Mki67* transcript (**Fig. 4b**). However, Ki67 expression was absent in Mfsd2a$^+$ cEC and αSMA$^+$ CD31$^+$ aEC in control and disease (**Fig. 4d-f**).

To test whether the formation of neo-vessels from vECs increases vein density in the inflamed spinal cord during EAE, we quantified the fraction of the Vcam1$^+$ area within the vascular network as a readout of vein coverage. Vcam1$^+$ area was significantly higher in acute (~7.5%) and to a lesser extent in chronic (~4%) EAE spinal cords relative to CFA (~1.5%; **Fig. 4g**). The lower vein density observed in chronic EAE could be explained, in part, by sequential specification of a venous (acute) followed by capillaries and/or arterial fate (chronic) during disease, similar to either postnatal CNS brain angiogenesis, or pathological angiogenesis in the retina[61-63].

228 DE analysis of diseased versus control vECs showed that the top upregulated transcripts in
229 both acute and chronic EAE were angiogenesis and tip cell markers (**Fig. 3e**). To validate these
230 scRNAseq findings *in vivo*, we analyzed expression of several angiogenic/tip cell markers (*Egfl7*,
231 Mcam, *Ecm1*, *Serpine1*, and Emcn) in spinal cords by fluorescent *in situ* hybridization (FISH) and
232 immunofluorescence staining (IF). Epidermal growth factor-like 7 (Egfl7) is an ECM-associated
233 protein that promotes angiogenesis in multiple organs including postnatal brain and retina[64-67]. DE
234 analysis of *Egfl7* expression by scRNAseq did not show a significant upregulation in diseased
235 relative to control vECs (**Fig. 5a**). However, assessment of *Egfl7* mRNA expression in spinal cord
236 tissue via FISH, combined with IF for the EC marker Caveolin-1, showed that *Egfl7* mRNA levels
237 are low-to-absent in CFA, but upregulated in inflamed blood vessels near white matter lesions in
238 acute EAE (**Fig. 5b-c;** data not shown). Melanoma cell adhesion molecule (Mcam), can function
239 either as a receptor for Wnt5a, Netrin1, FGF4, VEGF-C, and Wnt1[68], or co-receptor for VEGFR2
240 to bind VEGF-A[69] and promote angiogenesis. Its expression is enriched in proliferating ECs and
241 tip cells of the brain and retina[59]. DE analysis by scRNAseq showed significant upregulation of
242 *Mcam* mRNA in both acute and chronic EAE vECs (**Fig. 5d**). Mcam protein expression was
243 significantly upregulated in the inflamed veins in acute EAE relative to CFA *in vivo* (**Fig. 5e-f**).
244 Extracellular matrix protein 1 (Ecm1) is a secreted glycoprotein that exerts its angiogenic function
245 by potentiating epidermal growth factor receptor (EGFR) signaling [70], which in turn regulates the
246 synthesis and secretion of other angiogenic factors, including VEGF-A[71]. DE analysis revealed
247 that *Ecm1* mRNA was one of the most significantly upregulated genes in acute, and to a lesser
248 extent, chronic EAE (**Fig. 5g**). Assessment of *Ecm1* mRNA expression in control and EAE spinal
249 cord tissue corroborated these findings (**Fig. 5h-i**). The serine protease inhibitor Serpine1 is a
250 specific inhibitor of the plasminogen activation system[72] and plays a crucial role in tumor

progression and angiogenesis[73]. Expression of *Serpine1* was significantly upregulated in acute, and to a lesser extent, chronic EAE vEC clusters (**Fig. 5j**). Assessment of *Serpine1* RNA expression *in vivo* revealed a trend toward increased expression in inflamed white matter blood vessels in acute EAE relative to control ($p = 0.1261$; **Fig. 5k-l**). Endomucin (Emcn) is an integral membrane glycoprotein expressed in cECs and vECs[74] that modulates VEGF-induced angiogenesis in the developing retina[75]. DE analysis by scRNAseq revealed that *Emcn* expression was upregulated in EAE vECs (**Fig. 5m**), but downregulated in diseased cECs, further supporting the hypothesis that angiogenesis is unique to vECs in neuroinflammation. Assessment of Emcn protein confirmed increased expression in acute EAE spinal cord tissue, relative to control and chronic EAE (**Fig. 5n-o**).

In conclusion, the *in vivo* validation of select angiogenic/tip cell marker expression identified through scRNAseq suggests that neo-angiogenesis is likely highly upregulated in inflamed veins within white matter lesions during peak (acute) EAE and downregulated in the chronic phase of the disease.

Expression of several angiogenic markers is upregulated in human MS tissue

Previous studies have shown higher vessel density around acute and chronic MS plaques[76], where ECs have irregular morphology[20] and express some markers of proliferation[21]; yet the molecular signatures of pathological angiogenesis in human MS are unknown. We compared expression of several neo-angiogenesis markers, identified through scRNAseq in EAE, in acute or chronic demyelinating plaques from white matter (WM) lesions in 10 MS patients, to either normal appearing white matter (NAMW) from the same MS cases, or NAWM from brain samples of 10 non-neurological cases (**Supplementary table 5**) with immunohistochemistry, or *in situ*

hybridization. The CD31$^+$ vascular coverage (vessel density) was significantly higher inside the WM lesions compared to NAWM in MS subjects, or NAWM in non-neurological controls (**Fig. 6a-a"; d**), confirming prior findings[76]. Importantly, expression of two angiogenesis marker proteins upregulated in EAE, EGFL7 and MCAM, was also increased in blood vessels within demyelinating WM lesions of MS patients (**Fig. 6b-c"**). There was a 3-fold increase in vascular EGFL7 protein expression in WM lesions compared to adjacent NAWM in the same MS cases as well as those from non-neurological controls (**Fig. 6e**). In addition, there were significantly more MCAM$^+$ vessels both inside chronic lesions and in NAWM of MS patients compared to controls (**Fig. 6f**). Expression of mRNAs for two additional angiogenesis markers, *SERPINE1* and *ECM1*, showed a similar pattern to EGFL7 protein (**Extended Data Fig. 4a-c"**). Thus, several molecular markers of pathological angiogenesis identified through scRNAseq in EAE are also upregulated in demyelinating MS plaques from RRMS cases.

We then asked whether some of the markers of pathological neo-angiogenesis persist in SPMS, characterized by progressive neurodegeneration and cumulative disability. We examined expression of neo-angiogenesis markers in SPMS cases using spatial transcriptomics data from Kaufmann et al., 2022[77], which analyzed gene expression within an array of 100-µm diameter spots from MS lesions in SPMS. We binned all spots by their distance from MS lesion borders in each tissue type, using bins of 0.5 mm width, and calculated the fraction of spots within each bin where neo-angiogenesis genes were detected. White matter (WM) spots near MS lesions showed higher expression for both *SERPINE1 and MARKSL1* mRNAs compared to either gray matter (GM) area near the lesion, or a distant region (sulcus area; **Extended Data Fig. 4e, g**). In contrast, *EGFL7* and *ECM1* mRNAs showed higher expression in the GM near the lesion (**Extended Data**

Fig. 4d, f). Overall, this analysis revealed that molecular markers of pathological neo-angiogenesis are also present in SPMS.

Treatment with the anti-VEGF-A monoclonal antibody bevacizumab at the onset of EAE ameliorates disease course by downregulating transcriptomic features of pathological neo-angiogenesis

VEGF-A and TGF-β signaling pathways were highly upregulated in vECs together with features of neo-angiogenesis from acute and chronic EAE (**Fig. 3**), implicating them as potential drivers of angiogenesis in neuroinflammation. To test whether VEGF-A inhibition reduces transcriptomic features of neo-angiogenesis in EAE, we administered either bevacizumab (5mg/kg), a humanized anti-VEGF-A monoclonal antibody that binds to and prevents all VEGF-A isoforms from interacting with their receptors[32-34], or an IgG1 isotype control, to EAE mice starting from 7 d.p.i. (before disease onset) every 7 days until tissue collection at acute (16 d.p.i.; referred to as BevAc), and late chronic (40 d.p.i; referred to as BevCh) stages (**Fig. 7a**). Treatment with bevacizumab diminished the clinical course of EAE and resulted in lower incidence of death relative to IgG control (**Fig. 7b**). Although there was no significant difference in disease onset, the peak clinical score and the score on the day of collection were reduced in bevacizumab-treated mice (**Fig. 7c-e**). Since the EAE clinical outcomes depend on immune cell activation and CNS infiltration, we analyzed the number and activation of infiltrating immune cells in the spinal cords between BevAc and IgG - treated EAE mice by flow cytometry. The number of either MHC II^+ and $CD86^+$ dendritic cells (DCs), $CD11b^+$ neutrophils, the percentage of activated T cells ($CD44^{high}CD62L^{low}$), $CD4^+$ helper T cell subtypes and macrophages that infiltrated the spinal cords were similar between the BevAc - and IgG - treated EAE mice (**Extended Data Fig. 5**). Therefore,

the clinical benefits of the bevacizumab regimen used in our study were likely not mediated by alterations in immune cell activation or infiltration into the CNS.

To determine whether bevacizumab treatment suppresses the transcriptomic signatures of neo-angiogenesis in vECs during EAE, we isolated spinal cords ECs from BevAc mice for scRNAseq. BevAc ECs formed a separate cluster from both CFA and acute EAE samples; the arrangement of ECs in the t-SNE plot reflected the AV zonation observed previously (**Fig. 7f, g**). GSEA of differentially expressed genes revealed that bevacizumab treatment downregulated genes associated with angiogenesis, cell adhesion, EndoMT transition, as well as VEGF and TGF-β signaling (**Fig. 7h, Extended Data Table 2**). Interestingly, expression of several apoptosis genes (e.g., *Bcl10*, *Bclaf1*, *Bcl6*, *Bcl2*, etc.) was also downregulated in BevAc ECs, further corroborating the protective effects of bevacizumab on the CNS vasculature in EAE (**Extended Data Table 2**). DE analysis of BBB-specific genes showed that the tight junction (TJ) protein ZO-1 (*Tjp1*) was increased significantly in BevAC ECs (Fig 7i; **Extended Data Table 2**), suggesting that VEGF signaling may regulate specific aspects of BBB function (e.g. TJs).

Next, we examined whether neo-angiogenesis markers upregulated in acute EAE (*Egfl7*, Mcam, *Ecm1*, *Serpine1*, Emcn) showed changes in expression in BevAc ECs. While transcript levels of *Egfl7* were upregulated in BevAc ECs by scRNAseq, those for *Ecm1* and *Emcn* were significantly reduced in BevAc ECs compared to acute EAE ECs (**Fig. 8a, c, e**). *Mcam* and *Serpine1* transcripts showed a downward trend in BevAc ECs compared to acute EAE ECs (**Fig. 8b, d**). We validated these findings with FISH (*Egfl7*, *Ecm1*, *Serpine1*) and IF (Mcam, Emcn) *in vivo*. In spite of upregulated *Egfl7* expression in BevAc ECs with scRNAseq (**Fig. 8a**), *Egfl7* mRNA levels were significantly reduced in BevAc blood vessels compared to IgG -t reated acute EAE blood vessels *in vivo* by FISH (**Fig. 8f, f', k**). *Ecm1* and *Serpine1* mRNAs and Emcn protein

showed the same pattern *in vivo* as with scRNAseq with reduced expression in blood vessels from BevAc- compared to IgG -treated acute EAE spinal cords (**Fig. 8, c-e, h-j', m-o**). In contrast, the expression of Mcam protein was unaltered in spinal cord blood vessels from BevAc compared to IgG-treated EAE mice (**Fig. 8g, g', l**). Finally, there was a non-significant trend in decreased vein coverage in BevAc compared to IgG - treated acute EAE spinal cords (**Fig. 8p**).

A central features of pathological angiogenesis in cancer is the presence of unperfused blood vessels[29,53]. We injected fluorescently-labeled lectin intravenously in bevacizumab- or IgG - treated EAE mice at 40 d.p.i (chronic phase) to visualize unperfused vessels. There were many unperfused vessels around spinal cord lesions in IgG - treated EAE mice, but they were almost absent after bevacizumab treatment; however, the number of proliferating ECs was low-to-absent by chronic EAE regardless of treatment (**Extended Data Fig. 6a-b'**). We compared the number of lesions, extent of demyelination and endogenous IgG leakage (a measure of BBB permeability) between BevCh and IgG - treated EAE spinal cords. Although the number of lesions was similar between the two treatment groups, the percentage of demyelinated WM area (measured by the absence in fluoromyelin staining) was significantly reduced in BevCh compared to IgG - treated EAE spinal cords, largely because the lesion sizes were smaller (**Extended Data Fig. 6c-e'**). Interestingly, the average intensity of IgG leakage was not significantly different between BevCh and IgG - treated EAE spinal cords (**Extended Data Fig. 6c, c', f, f'**), suggesting that bevacizumab regimen did not reduce BBB leakage, consistent with its modest effects on BBB transcripts by scRNAseq (**Fig. 7i**). Overall, these data indicate that VEGF-A signaling drives pathological neo-angiogenesis in EAE from venous ECs; its blockade reduces pathological neo-angiogenic gene signatures and clinical outcome in EAE, independently of immune cell-mediated effects.

DISCUSSION

The presence of angiogenesis and high levels of VEGF-A has been documented in both MS and EAE for several decades[20-23,31]; previous functional studies using monoclonal antibodies to block VEGF-A signaling have also shown that VEGF-A-driven angiogenesis worsens EAE clinical outcomes[26,27]. However, the timing and relation of neo-angiogenesis to EAE/MS progression, its molecular characterization, and the vascular origin and signaling pathways driving neo-angiogenesis in neuroinflammation are poorly understood. Here, we employed scRNAseq and GSEA, together with fluorescent *in situ* hybridization and immunofluorescence validation to show that venous ECs, primarily in acute EAE, express transcriptomic signatures of neo-angiogenesis together with activation of pro-angiogenic VEGF-A and TGF-β signaling (**Fig. 3**). Thus, venous ECs are the primary EC subtype responsible for pathological angiogenesis in neuroinflammation (**Fig. 8q**). We find that expression of several neo-angiogenesis markers, identified from scRNAseq in EAE, is also upregulated in human MS lesions from either RRMS or SPMS cases in addition to increased vascular density (**Fig. 6; Extended Data Fig. 4**). Finally, through functional validation studies, we show that blockade of VEGF-A signaling with bevacizumab improves EAE clinical outcomes by inhibiting signatures of pathological neo-angiogenesis, without significantly affecting immune cell activation (**Figs. 7, 8**). Below, we discuss a putative model for pathological angiogenesis in neuroinflammation and potential therapeutic implications for MS.

Although previous studies employing bulk or scRNAseq of the endothelium in EAE have shown that ECs acquire transcriptomic features of inflammation and lose expression of those associated with the BBB[45,46], our scRNAseq and validation data have revealed, for the first time, that the transcriptomic signatures of angiogenesis arise from vein/venule ECs in neuroinflammation. This was possible since we isolated sufficient ECs from each vessel subtype

in healthy, CFA controls and disease states to identify gene signatures and pathways that were up- and downregulated in neuroinflammation. Since the number of angiogenic ECs arising from vEC/vnECs is small, they were likely missed in previous analyses[45,46]. Nevertheless, the identification of vECs as the source of neuroinflammation-related angiogenesis is somewhat surprising. The classical model suggests that angiogenesis occurs from pre-existing capillaries, whereby cECs respond to a hypoxia-induced VEGF-A gradient and differentiate into migratory tip and proliferating stalk cells that expand the vascular network (reviewed in [78,79]). Several recent studies have challenged this dogma. Coelho-Santos *et al*. have shown that CNS angiogenesis in the neonatal mouse brain is initiated exclusively from cortical ascending venules[61]. Lee *et al*. have utilized EC vascular subtype-specific inducible reporter mice to fate map ECs in the developing postnatal retinal vasculature, and discovered that ~80% of ECs are of venous origin at both P7 and P25[63]. Moreover, neo-angiogenic sprouts arise exclusively from veins in the oxygen-induced retinopathy (OIR) model[63]. Rohlenova *et al.* have employed scRNAseq and trajectory inference to predict that vECs differentiate into neo-angiogenic tufts during choroidal neovascularization (CNV), a model for wet age-related macular degeneration (AMD)[80]. Their data also suggests that disease-specific EC population, which contains clusters of proliferating and tip ECs, exhibit vein marker expression[80]. Lastly, a recent scRNAseq study of the lung tumor vasculature has also found that tumors have a higher proportion of vECs, compared to the normal vasculature[57].

Why are venous/venule, but not arterial/capillary ECs angiogenic in neuroinflammation? Postcapillary venules and veins are the primary sites of immune cell infiltration and BBB damage in MS/EAE[1,2]. Activated T cells that infiltrate into the hypoxic CNS parenchyma secrete VEGF-A[81,82], which can promote angiogenesis locally (**Fig. 8q**). Macrophages, which make up a large proportion of cellular infiltrates in MS/EAE also secrete numerous pro-angiogenic factors,

411 including VEGF-A, FGF, PDGF and Angiopoetin-1 and -2[83] (**Fig. 8q**). They also produce the
412 matrix metalloproteinases MMP-7 and -9[84], which can digest the ECM surrounding the
413 veins/venules to free ECM-bound VEGF-A, while simultaneously creating a path through the
414 vascular basement membrane for EC migration. Another explanation for the venous origin of neo-
415 angiogenesis in neuroinflammation could be related to differences in shear stress levels present in
416 arteries, capillaries and veins. Phosphorylation of VEGFR2, VE-Cadherin, CD31 and Erk1/2 is
417 regulated by shear stress (reviewed in[85]). High shear stress in arteries may obstruct EC proliferation
418 and migration, whereas low shear stress in veins may be conducive to angiogenesis.

419 Our scRNAseq analyses of spinal cords ECs from control and EAE mice revealed that gene
420 sets associated with VEGF, but not Wnt/β-catenin, signaling and neo-angiogenesis are specifically
421 enriched in vECs in neuroinflammation (**Fig. 3**), implicating VEGF-A as a possible driver of neo-
422 angiogenesis in EAE (**Fig. 8q**). Previous studies have shown that administration of VEGF-A
423 inhibitors such as bevacizumab [26], B20-4.1.1[27] or SU5416[24] improve clinical outcomes in EAE
424 mice. It has been unclear, however, if VEGF inhibitors exert their therapeutic effects directly on
425 CNS angiogenesis in neuroinflammation, or indirectly by dampening the peripheral immune
426 response resulting in less CNS immune infiltration. Treatment with SU5416 (Semaxinib), a potent
427 and selective inhibitor of VEGFR2, reduces immune filtration in the CNS [24]. Similarly, Macmillan
428 *et al.*, have shown that prophylactic administration of bevacizumab (humanized monoclonal
429 antibody) and B20-4.1.1 (monoclonal antibody that binds both human and mouse VEGF-A) prior
430 and throughout EAE onset in mice reduces peripheral T cell responses, decreases $CD4^+$ T cell
431 recruitment into the spinal cord and IL-17A and IFNγ secretion in response to *in vitro* stimulation
432 with MOG_{35-55} [26,27]. However, the authors did not assess activation, differentiation, and CNS
433 infiltration of various immune cell subtypes such as dendritic cells, monocytes, macrophages and

neutrophils. Although, it has been suggested that bevacizumab does not bind murine VEGF-A, our study confirm previous observations[26] that its administration improves EAE clinical outcomes. Moreover, we find that therapeutic administration of bevacizumab, a day before EAE onset, does not affect immune cell activation or their CNS infiltration, but reduces transcriptomic features of neo-angiogenesis and VEGF-A signaling by both scRNAseq and FISH *in vivo* validation studies (**Figs 7, 8; Extended Data Figure 5**). GSEA analysis of BevAc ECs revealed significant downregulation of pro-angiogenic genes that were upregulated in acute EAE. We found significant downregulation of *Egfl7*, *Ecm1*, *Serpine1* and Emcn in the vasculature of bevacizumab-treated mice relative to IgG-treated controls by FISH and IF, corroborating that expression of these pro-angiogenic genes may be regulated by VEGF-A signaling. Bevacizumab also reduces the number of unperfused vessels, a key hallmark of pathological angiogenesis. The effects of bevacizumab treatment are more modest in our hands than prior reports[26]. Since our treatment regimen started at 7 d.p.i, we may have targeted primarily angiogenesis, rather than a combined effect on angiogenesis and immune cell suppression seen when bevacizumab is administered profilactically, or our dosing regimen may have been suboptimal to achieve complete VEGF-A suppression.

Vcam1 primarily functions as an immune cell adhesion molecule on ECs [86], and VEGF-A is known to induce endothelial Vcam1 expression during inflammation [87]; however, Vcam1 is also a marker of venous cell fate. This could confound our conclusions that vein density is increased in acute neuroinflammation and bevacizumab treatment reduces vein coverage. Our scRNAseq data show that while *Vcam1* levels are significantly upregulated in acute EAE ECs, the proportion of vECs expressing it remains the same (**Extended Data Table 1**; Sheet 7), suggesting that vECs express *Vcam1* in both control and EAE settings. scRNAseq analysis also revealed that treatment with bevacizumab did not significantly alter *Vcam1* expression levels in BevAc ECs relative to

untreated acute EAE ECs. Overall, these observations support our conclusions that Vcam1^{+} vessel coverage is a reliable method to measure changes in vein density in neuroinflammation.

In addition to its role in angiogenesis, VEGF-A is a key regulator of vascular permeability. Activation of VEGF signaling downregulates expression of Claudin-5 and Occludin[88], induces phosphorylation of Occludin and ZO-1[89,90] and disrupts ZO-1 and Occludin organization[91], resulting in TJ disassembly in brain microvascular endothelial cells (BMECs). VEGF also promotes VE-cadherin endocytosis and barrier dysfunction[92]. DE analysis revealed that expression of the TJ protein, ZO-1 (*Tjp1*), was significantly upregulated in BevAc ECs, likely due to inhibition of VEGF signaling[93]. It is possible that VEGF-A inhibition in EAE may reduce both EC neo-angiogenesis and promote BBB function. However, expression of *Cldn5* and *Ocln* mRNAs was unchanged in BevAC compared to untreated acute EAE ECs and there was no change in serum IgG leakage (**Extended Data Fig. 5**) indicating that our bevacizumab regimen likely exerts its therapeutic effects through inhibition of VEGF-A-mediated angiogenesis.

In conclusion, our study suggests a model in which VEGF-A derived from either reactive astrocytes[94] or infiltrating immune cells induces neo-angiogenesis from vein ECs in EAE/MS through upregulation of several angiogenic markers such as Egfl7, Emcn, Ecm1, Serpine1 and Mcam (**Fig. 8q**). Inhibition of VEGF signaling with bevacizumab results in amelioration of EAE disease course, likely through a reduction in neo-angiogenesis (including downregulation of Egfl7, Emcn and Ecm1), without affecting immune cell activation or CNS infiltration (**Fig. 8q**). Several markers of pathogenic angiogenesis identified through our scRNAseq in EAE are also upregulated in either acute or chronic demyelinating MS plaques in RRMS or in SPMS cases, through *in situ* hybridization analysis and post-hoc spatial transcriptomic analysis of published data[77], respectively. SPMS is characterized by progressive neurodegeneration and cumulative disability

with no current treatment. Our results advocate for VEGF inhibition as a possible therapeutic intervention in the early phases of EAE/MS, to reduce the pathological effects of neo-angiogenesis in disease maintenance and progression, and improve long-term neurological deficits in patients as they transition to SPMS.

Online Methods

Mice

All experiments were approved by the Institutional Animal Care and Use Committees (IACUC) at Columbia University Irving Medical Center. Animals used for breeding and EAE induction were housed in sex-matched cages of up to five mice in the vivarium with access to food and water *ad libitum*. Wild-type C57BL/6J, obtained from the Jackson Laboratory (Maine), were used for EAE experiments to collect spinal cords from CFA control, acute and chronic EAE for analysis of neo-angiogenesis via immunofluorescence and RNA fluorescent in situ hybridization (FISH). TCF/LEF::H2B::eGFP (Wnt reporter) mice[9,41], purchased from Jackson Laboratory, were used for single-cell RNA sequencing (scRNAseq) of control and EAE spinal cord endothelial cells (ECs), to track Wnt/β-catenin pathway activation in ECs post hoc within the RNAseq data. The mice were genotyped for GFP with primers [CCCTGAAGTTCATCTGCACCAC (forward); TTCTCGTTGGGGTCTTTGCTC (reverse)] as described[41].

Induction of MOG_{35-55} EAE

The induction of MOG_{35-55} EAE in mice has been described[9,41]. Briefly, 10–12-week-old female mice were immunized by subcutaneous injection with 100 μg of myelin oligodendrocyte

glycoprotein 35-55 (MEVGWYRSPFSRVVHLYRNGK-COOH) in complete Freund's adjuvant (CFA) containing 200 μg heat killed mycobacterium tuberculosis H37Ra (Difco). 400 ng of *Bordetella pertussis* toxin was administered intravenously at day 0 and day 2. Mice were examined for clinical EAE signs starting at 5 days post immunization (d.p.i) using the scale (0.5-point gradations for intermediate presentation): 0, no signs; 1, flaccid tail; 2, hindlimb paresis; 3, hindlimb paralysis; 4, hindlimb and forelimb paralysis; 5, moribund; 6, death. Control animals immunized with CFA emulsion and pertussis toxin did not exhibit any clinical signs. Spinal cord tissue was collected at the peak acute (16 d.p.i), the beginning of chronic (28 d.p.i), or chronic (40 d.p.i) EAE, as well as from healthy and CFA controls, for scRNAseq and immunofluorescence/RNA *in situ* hybridization analysis of angiogenic marker expression.

Injection of VEGF monoclonal antibodies in EAE

Mice induced with MOG_{35-55} EAE were placed into two groups at 7 d.p.i.: Group 1 (bevacizumab-treated) was injected intraperitoneally with 5 mg/kg of the anti-VEGF monoclonal antibody, bevacizumab (Selleckchem, Cat. # A2006) every 7 days until tissue collection at 40 d.p.i. Group 2 (IgG-treated) was injected with 5 mg/kg of the immunoglobulin G isotype control ([IgG] Biolegend, Cat. # 403502) every 7 days until tissue collection at 40 d.p.i. (**Figure 7a**). Spinal cords were collected for analysis of angiogenic markers by either immunofluorescence, or FISH. Bevacizumab-treated mice were also collected at the acute EAE (16 d.p.i) for immune cell profiling and scRNAseq.

Immune cell profiling in EAE

Flow cytometry was used to quantify changes in the immune profile in the periphery and spinal cords at acute EAE. Antibodies used for this analysis are listed in **Supplementary Table 3**.

527 Bevacizumab- or IgG-treated EAE mice (16 d.p.i.) and healthy controls were anesthetized with
528 isoflurane and perfused briefly with sterile PBS. Spinal cords were dissected into DMEM on ice
529 and dissociated through a 40 μm nylon mesh cell strainer with the back of a 10 ml syringe plunger.
530 Cells were collected from the interface of a 30%-70% Percoll gradient. Spleens were dissociated
531 through a 40 μm nylon mesh cell strainer with a 1 mL syringe plunger. Splenocytes were treated
532 with 3 mL red blood cell lysis buffer (155 mM NH_4Cl, 10 mM $KHCO_3$, 0.1 mM EDTA) for five
533 minutes at room temperature and processed for analysis.

534 For T cell analysis, half of each sample was used for cytokine staining as described[9]. Cells
535 were stimulated *in vitro* with 500x Cell Stimulation Cocktail (eBiosciences; 00-4975-03) diluted
536 to 1x in T cell media (RPMI with 10% fetal bovine serum, 1x penicillin/streptomycin, 1x
537 glutamine, 1x non-essential amino acids, and 50 μM β-mercaptoethanol) for 4 hours at 37 °C.

538 Cells were washed with FACS buffer, transferred to a 96-well plate and blocked in
539 CD16/CD32 Fc block (BD Biosciences, 553141) diluted 1:200 in FACS buffer for 15 minutes on
540 ice. Cells were washed, then stained with surface marker antibodies and Live/Dead Aqua
541 (ThermoFisher, L34965, 1:1000 dilution) for 1 hour on ice. Cells were then fixed and
542 permeabilized with BD Cytofix/Cytoperm (BD Biosciences, 554722) for 25 minutes on ice,
543 washed with 1x permeabilization solution and stored in FACS buffer overnight. The following
544 day, intracellular cytokines staining was performed in permeabilization solution; cells were then
545 resuspended in FACS buffer for analysis. For myeloid cell analysis, samples were not stiumulated,
546 but were incubated with Fc block directly after dissociation, then stained for surface antigens, and
547 fixed, as described above.

548 Samples for both panels were analyzed on a Novocyte Quanteon (Agilent) equipped with
549 405 nm, 488 nm, 561 nm, and 640 nm lasers at the Columbia Stem Cell Initiative Flow Cytometry

Core. Compensation beads [Anti-Rat Ig, κ/Negative Control (BD Biosciences, 552844) or UltraComp eBeads Plus (ThermoFIsher, 01-3333-41), depending on host species] were used for single color controls. Gates were set using fluorescence minus-one controls on tissue-matched cells. Compensation and analysis were performed with FlowJo software (Becton Dickinson & Company, version 5.0).

Isolation of endothelial cells from control and EAE spinal cords

Mice were anesthetized with isoflurane and perfused for 4 minutes with ice-cold sterile PBS. The spinal cord was dissected into Earl's balanced salt solution (EBSS) and dissociated into a single cell suspension using an established protocol[95]. The single cell suspension was resuspended in 200 µl of CD16/CD32 Fc block (BD Biosciences, Cat. # 553141; 1/200 in FACS buffer) and incubated at room temperature for 15 minutes. Samples were washed with 2 ml of FACS buffer, and 100 µl were kept aside for unstained and fluorescence minus one (FMO) controls. The cells were resuspended in 200 µl of anti-CD31-APC (Biolegend, Cat. # 102410; 1/200 in FACS buffer) antibody to label endothelial cells (ECs) and incubated on ice in the dark for 30-60 mins. Following antibody labeling, the samples were washed twice with 2 ml of FACS buffer and resuspended in 400 µl of propidium iodide (Thermofisher, Cat. # P1304MP; 1/10,000 in FACS buffer). Gates for the surface stain were set using the unstained and FMO controls. The CD31-APC positive ECs were sorted out using the BD FACS Aria Flow Cytometer (Columbia Stem Cell Initiative Flow Cytometry Core) and processed for scRNAseq.

Single-cell RNA sequencing analysis

For single-cell RNA sequencing (scRNAseq), the 10x Genomics Chromium[96,97] platform was used to generate low-depth data (~2000 genes/cell), which was processed using the Cell Ranger analysis pipeline to align reads and generate feature-barcode matrices. The Seurat R package[42] was implemented to read the output of the Cell Ranger pipeline and merge cells from all the samples (controls and EAE) into a single R object. The standard pre-processing workflow for scRNAseq data was carried out in Seurat, which consisted of the selection and filtration of cells based on quality control metrics (e.g., number of unique genes detected in each cell > 200, total number of molecules detected within a cell > 1,000 and < 50,000, percentage of reads within a cell that map to the mitochondrial genome < 20, etc.), data normalization and scaling, and the detection of highly variable features. Next, linear dimensionality reduction (PCA) was performed on the scaled data using the previously determined highly variable features (2,000 genes), an alternative heuristic method ('Elbow plot') was implemented to determine the 'dimensionality' of the dataset, and cells were clustered by applying the weighted shared nearest-neighbor graph-based clustering method[98] using the first 30 PCs. Lastly, the 30 PCA dimensions were further reduced into two-dimensional space using the non-linear dimensional reduction technique, t-distributed stochastic neighbor embedding (t-SNE), to visualize and explore the scRNAseq dataset and each of its unique EC clusters.

Differential Gene Expression Analysis

The Seurat “FindMarkers” function with the default Wilcoxon Rank Sum test was implemented to compile the lists of differentially expressed genes, by comparing expression profiles of disease enriched (acute and chronic) EC clusters to control EC clusters, and BevAc EC clusters to untreated acute EAE EC clusters.

Gene Set Enrichment Analysis (GSEA)

To assess changes in putative cell type composition and signatures, the proportion of cells in each cluster was calculated and chi-squared tests were performed to estimate differences in cell type composition. Differential gene expression (DE) analysis was run on each cluster (using DESeq, SCDE R and IPA pathway packages) with experimental condition as the group identity to discern variations in gene expression[99] and highlight which clusters have further heterogeneity associated with each condition. Following DE analysis, a score was calculated for each gene using the formula: Gene score = $-\log_{10}(\text{pval})$ x sign ($\log_2$fc). Up- and downregulated genes had a positive and negative score, respectively. The numeric value of the gene score was inversely correlated with the degree of significance, that is, genes that had the highest statistically significant difference in expression and the lowest p-values had the highest score, while non-significant genes with high p-values had a correspondingly low gene score. This score was used to rank each gene in DE gene list (**Extended Data Table 1**). New gene sets relevant to pathways, processes and cell types of interest (VEGF signaling, canonical Wnt/β-catenin signaling, non-canonical Wnt signaling, chemokine/cytokine signaling, TGF-β signaling, extracellular matrix, cell-cell adhesion, transporters, Notch signaling, angiogenesis, endothelial cell proliferation, endothelial cell migration, apoptosis, antigen processing and presentation, blood-brain barrier, inflammation, endothelial-to-mesenchymal transition, tip cells) were compiled as part of the overall gene set enrichment analysis (**Extended Data Table 1, Sheet 1)**, using the GO, KEGG, DAVID and GSEA databases as published before[100-102]. The ranked list of DE genes, along with the compiled gene sets, were loaded onto GSEA 4.1.0 software, and run through 'GseaPreranked' with the following settings: Number of permutations = 1,000; Collapse/Remap to gene symbols = No_collapse; Max

size: exclude larger sets = 1,500; all other settings were left at 'default'. Gene sets with FDR q-value ≤ 0.10 were deemed significantly enriched (na_pos) or depleted (na_neg) in the cluster of interest (e.g., acute, or chronic EAE EC enriched cluster) relative to its counterpart (e.g., control EC enriched cluster) in the DE analysis, and plotted in the GSEA graphs.

Immunofluorescence analysis

Mice used for immunofluorescence staining were anesthetized with isoflurane and perfused with PBS for 4 minutes followed by 4% PFA for 6 minutes. Spinal cords were extracted and post-fixed for 2 hours, washed three times in PBS for 30 minutes, then cryoprotected in 30% sucrose overnight and embedded in Tissue Plus O.C.T. Compound (Fisher Scientific, Cat # 4585). The tissue blocks were stored at -80 °C until use. Tissues were then sectioned at 12 µm on a Leica cryostat and stored at -80 °C until use. For staining, slides were air-dried for 20 minutes then placed horizontally in a humidified chamber. Slides were washed once in PBS for 10 minutes to remove excess OCT, then blocked for 1 hour in blocking buffer (10% BSA, 0.1% Triton-X-100 in 1x PBS). Primary antibodies (**Supplementary Table 4**) were diluted in 0.1% Triton-X-100 in PBS with 1% BSA. Primary antibody solutions were incubated overnight at 4 °C. Slides were washed three times for ten minutes with PBST (0.1% Triton-X-100 in PBS), then primary antibodies were targeted using associated fluorescently tagged secondary antibodies (1:1000 for Alexa488 and Alexa594, 1:500 for Alexa647). Secondary antibodies were diluted in PBST and incubated for two hours at room temperature. Nuclei were then labeled with DAPI (4′,6-diamidino-2-phenylindole, 1:20,000 in PBST) for 10 minutes, then slides were washed twice with PBST and twice with PBS. Slides were mounted with Vectashield (Vector Labs, Cat # H-1000), coverslipped and sealed with

clear nail polish, and stored at -20 °C. Imaging of brain sections were performed with either a Zeiss LSM700 confocal microscope or a Zeiss AxioImager.

Chromogenic immunohistochemistry of human tissue

Formalin-fixed human brain samples were obtained from the NIH Brain & Tissue Repository-California, Human Brain & Spinal Fluid Resource Center VA West Los Angeles Healthcare Center, Los Angeles, California, which is supported in part by National Institutes of Health and the US Department of Veterans Affairs under the IRB protocol # AAAQ7343. Brain tissues from 10 MS and 10 non-neurological control patients were used in this study (see **Supplementary Table 5**). Upon receipt, the fixed samples were washed with cold PBS then dehydrated in 30% sucrose before embedding in Tissue-Tek O.C.T. Compound (Sakura; Torrance, CA) and cryosectioned 12 μm thick. Single target immune-peroxidase staining was performed as described[41]. Hematoxylin counterstain was used for all stains except for CD31. For 2-target immune-peroxidase staining, targeting both CD31 and Ki67, the ImmPRESS Duet Double Staining Polymer kit (Vector Labs, Cat. # MP-7724, Burlingame, CA) was used, according to manufacturer's recommendations. No nuclear counterstain was used in these experiments. All primary antibodies were diluted in 1% bovine serum albumin, 0.1% Triton-X, in PBS. Images were acquired with a Zeiss Axioimager using a color camera and 10X objective.

***In situ* hybridization**

Digoxigenin-labeled probes were synthesized from plasmids obtained from TransOMIC using the Roche Applied Science *in vitro* transcription kit (Sigma, 11175025910). The probes used for these experiments are listed in **Supplementary Table 6**. Mice used for *in situ* hybridization experiments

were perfused with PBS only, brains and spinal cords were dissected out, embedded in OCT and frozen on dry ice, then stored at -80 °C. Sections were cut onto glass slides using a cryostat. Alkaline Phosphatase *in situ* hybridizations and fluorescent *in situ* hybridization (FISH) combined with immunofluorescence for vascular markers were performed as previously described[41,103]. Slides were imaged either on a Zeiss AxioImager, or an Zeiss LSM700 confocal microscope.

Image analysis

Images were prepared and analyzed using ImageJ/FIJI software. For fluorescence measurements, at least three sections were imaged per sample, and in each case, multiple (8-12) representative regions of interest (ROIs) were acquired using the confocal microscope (20x objective). For each ROI, multiple Z-stacks were acquired, and maximal projection was performed in ImageJ to properly capture the full depth of the CNS blood vessels. Background correction was performed in ImageJ when required. For statistical analysis, the mean value for each animal was calculated as the mean signal from all acquired ROIs.

Analysis of vein EC proliferation and vein density: Spinal cord tissue sections were stained with the proliferation marker, Ki67, vein marker, Vcam1, and nuclei marker, DAPI (**Supplementary Table 4**). Ki67-positive vein nuclei were counted and normalized to the total number of vein nuclei to get a readout of EC proliferation rate. ImageJ/FIJI was used to quantify the area of coverage by Vcam1-positive vessels to get a readout of vein density.

Analysis of angiogenic marker expression: Spinal cord tissue sections were analyzed for the expression of angiogenic markers (Egfl7, Mcam, Serpine1, Ecm1, Emcn) and vessel/vein marker (Caveolin-1/Vcam1) with either FISH combined with immunofluorescence or immunofluorescence staining. The vessel area was outlined by signal thresholding using the

ImageJ/FIJI software, and the mean fluorescence intensity (M.F.I.) of angiogenic marker expression within the vasculature was measured using the histogram analysis feature.

Statistical analyses

Statistical analyses of EAE disease course and parameters (day of disease onset, peak disease score and score on the day of collection), vascular subtype cell proportions within the scRNAseq data, vein EC proliferation and vein density, angiogenic marker expression and flow cytometry data were performed using GraphPad Prism. Gene set enrichment analysis was performed using the GSEA v4.1.0 Mac App. Data were analyzed by Student's t-test, one-way, two-way, or repeated measures (RM) ANOVA followed by Sidak's, Tukey's, or Bonferroni's post-hoc corrections. Significance (α) was set at 0.05. Data in the dotted bar graphs are represented as mean ± SEM, where each dot is the mean value from each animal.

Data availability

The raw and analyzed mouse endothelial scRNAseq datasets supporting this manuscript are archived at the NIH GEO repository under accession number GSE210776.

Acknowledgements

We thank Jeroen Bastiaans at Weill Cornell Medical College, New York for help with some experiments, Tyler Cutforth for advice with the preparation of mRNA probes and FISH experiments, Michael Kissner at the Columbia Stem Cell Initiative Flow Cytometry Core and Erin Bush at the Columbia Single Cell RNA sequencing facility for their advice and help with FACS isolation and single cell RNA sequencing experiments, respectively.

Author Contributions

Conceptualization: S.S., V.M., D.A.; Methodology: S.S., V.M., D.A.; Software: S.S., C.W., V.M.; Validation: S.S.; Formal analysis: S.S., M.Z.P., M.D.G, C.R.W, G.P.; Investigation: S.S., S.B., M.Z.P., M.D.G, C.R.W, G.P.; Resources: V.M., D.A.; Data curation: S.S., V.M., D.A.; Writing - original draft: S.S., S.B., C.W., V.M., D.A.; Writing & editing: S.S., S.B., C.W., V.M., D.A.; Visualization: S.S.; Supervision: V.M., D.A.; Project administration: D.A.; Funding acquisition: V.M., D.A.

COMPETING INTERESTS

The authors declare that the research was conducted without any commercial or financial relationships that can be construed as potential conflicts of interest.

FUNDING

Sanjid Shahriar, Saptarshi Biswas, Charlotte Wayne, Michael Glendinning, Vilas Menon and Dritan Agalliu are supported by grants from the NIH/NIMH (R01 MH112849), NIH/NINDS (R01 NS107344; R21 NS118891) and the National Multiple Sclerosis Society (RG-1901-33218).

MATERIALS AND CORRESPONDENCE

The materials are available upon request to Dritan Agalliu.

REFERENCES

1 Daneman, R. & Engelhardt, B. Brain barriers in health and disease. *Neurobiology of disease* **107**, 1-3 (2017).

2 Liebner, S. *et al.* Functional morphology of the blood-brain barrier in health and disease. *Acta Neuropathol* **135**, 311-336, doi:10.1007/s00401-018-1815-1 (2018).

3 Kirk, J., Plumb, J., Mirakhur, M. & McQuaid, S. Tight junctional abnormality in multiple sclerosis white matter affects all calibres of vessel and is associated with blood-brain barrier leakage and active demyelination. *The Journal of pathology* **201**, 319-327 (2003).

4 Pan, W., Banks, W. A., Kennedy, M. K., Gutierrez, E. G. & Kastin, A. J. Differential permeability of the BBB in acute EAE: enhanced transport of TNT-alpha. *The American journal of physiology* **271**, E636-642 (1996).

5 Brown, A., McFarlin, D. E. & Raine, C. S. Chronologic neuropathology of relapsing experimental allergic encephalomyelitis in the mouse. *Laboratory investigation; a journal of technical methods and pathology* **46**, 171-185 (1982).

6 Alvarez, J. I. *et al.* Focal disturbances in the blood-brain barrier are associated with formation of neuroinflammatory lesions. *Neurobiol Dis* **74**, 14-24, doi:10.1016/j.nbd.2014.09.016 (2015).

7 Lossinsky, A. S., Badmajew, V., Robson, J. A., Moretz, R. C. & Wisniewski, H. M. Sites of egress of inflammatory cells and horseradish peroxidase transport across the blood-brain barrier in a murine model of chronic relapsing experimental allergic encephalomyelitis. *Acta Neuropathol* **78**, 359-371 (1989).

8 Maggi, P. *et al.* The formation of inflammatory demyelinated lesions in cerebral white matter. *Ann Neurol* **76**, 594-608, doi:10.1002/ana.24242 (2014).

9 Lutz, S. E. *et al.* Caveolin1 is required for Th1 cell infiltration, but not tight junction remodeling, at the blood-brain barrier in autoimmune neuroinflammation. *Cell reports* **21**, 2104-2117 (2017).

10 Plumb, J., McQuaid, S., Mirakhur, M. & Kirk, J. Abnormal endothelial tight junctions in active lesions and normal-appearing white matter in multiple sclerosis. *Brain pathology (Zurich, Switzerland)* **12**, 154-169 (2002).

11 Kermode, A. G. *et al.* Breakdown of the blood-brain barrier precedes symptoms and other MRI signs of new lesions in multiple sclerosis. Pathogenetic and clinical implications. *Brain : a journal of neurology* **113 (Pt 5)**, 1477-1489 (1990).

12 Reijerkerk, A. *et al.* Tissue-type plasminogen activator is a regulator of monocyte diapedesis through the brain endothelial barrier. *Journal of immunology (Baltimore, Md. : 1950)* **181**, 3567-3574 (2008).

13 Winger, R. C., Koblinski, J. E., Kanda, T., Ransohoff, R. M. & Muller, W. A. Rapid remodeling of tight junctions during paracellular diapedesis in a human model of the blood-brain barrier. *Journal of immunology (Baltimore, Md. : 1950)* **193**, 2427-2437, doi:10.4049/jimmunol.1400700 (2014).

14 Aube, B. *et al.* Neutrophils mediate blood-spinal cord barrier disruption in demyelinating neuroinflammatory diseases. *Journal of immunology (Baltimore, Md. : 1950)* **193**, 2438-2454, doi:10.4049/jimmunol.1400401 (2014).

15 Abadier, M. *et al.* Cell surface levels of endothelial ICAM-1 influence the transcellular or paracellular T-cell diapedesis across the blood-brain barrier. *European journal of immunology* **45**, 1043-1058, doi:10.1002/eji.201445125 (2015).

16 Lake, B. B. *et al.* Integrative single-cell analysis of transcriptional and epigenetic states in the human adult brain. *Nature Biotechnology* **36**, 70-80, doi:10.1038/nbt.4038 (2018).
17 Biswas, S., Cottarelli, A. & Agalliu, D. Neuronal and glial regulation of CNS angiogenesis and barriergenesis. *Development* **147**, dev182279 (2020).
18 Girolamo, F., Coppola, C., Ribatti, D. & Trojano, M. Angiogenesis in multiple sclerosis and experimental autoimmune encephalomyelitis. *Acta neuropathologica communications* **2**, 1-17 (2014).
19 Lengfeld, J., Cutforth, T. & Agalliu, D. The role of angiogenesis in the pathology of multiple sclerosis. *Vascular cell* **6**, 1-6 (2014).
20 Proescholdt, M. A., Jacobson, S., Tresser, N., Oldfield, E. H. & Merrill, M. J. Vascular endothelial growth factor is expressed in multiple sclerosis plaques and can induce inflammatory lesions in experimental allergic encephalomyelitis rats. *Journal of neuropathology and experimental neurology* **61**, 914-925 (2002).
21 Holley, J. E., Newcombe, J., Whatmore, J. L. & Gutowski, N. J. Increased blood vessel density and endothelial cell proliferation in multiple sclerosis cerebral white matter. *Neurosci Lett* **470**, 65-70, doi:10.1016/j.neulet.2009.12.059 (2010).
22 Seabrook, T. J. *et al.* Angiogenesis is present in experimental autoimmune encephalomyelitis and pro-angiogenic factors are increased in multiple sclerosis lesions. *J Neuroinflammation* **7**, 95, doi:10.1186/1742-2094-7-95 (2010).
23 Kirk, S. L. & Karlik, S. J. VEGF and vascular changes in chronic neuroinflammation. *J Autoimmun* **21**, 353-363 (2003).
24 Roscoe, W. A., Welsh, M. E., Carter, D. E. & Karlik, S. J. VEGF and angiogenesis in acute and chronic MOG((35-55)) peptide induced EAE. *J Neuroimmunol* **209**, 6-15, doi:10.1016/j.jneuroim.2009.01.009 (2009).
25 Boroujerdi, A., Welser-Alves, J. V. & Milner, R. Extensive vascular remodeling in the spinal cord of pre-symptomatic experimental autoimmune encephalomyelitis mice; increased vessel expression of fibronectin and the alpha5beta1 integrin. *Exp Neurol* **250**, 43-51, doi:10.1016/j.expneurol.2013.09.009 (2013).
26 MacMillan, C. J. *et al.* Bevacizumab diminishes experimental autoimmune encephalomyelitis by inhibiting spinal cord angiogenesis and reducing peripheral T-cell responses. *J Neuropathol Exp Neurol* **71**, 983-999, doi:10.1097/NEN.0b013e3182724831 (2012).
27 MacMillan, C. J. *et al.* Murine experimental autoimmune encephalomyelitis is diminished by treatment with the angiogenesis inhibitors B20-4.1. 1 and angiostatin (K1-3). *PLoS One* **9**, e89770 (2014).
28 Matsumoto, K. & Ema, M. Roles of VEGF-A signalling in development, regeneration, and tumours. *The Journal of Biochemistry* **156**, 1-10 (2014).
29 Carmeliet, P. VEGF as a key mediator of angiogenesis in cancer. *Oncology* **69**, 4-10 (2005).
30 Campochiaro, P. A. Molecular pathogenesis of retinal and choroidal vascular diseases. *Progress in retinal and eye research* **49**, 67-81 (2015).
31 Su, J. J. *et al.* Upregulation of vascular growth factors in multiple sclerosis: correlation with MRI findings. *Journal of the neurological sciences* **243**, 21-30 (2006).
32 Presta, L. G. *et al.* Humanization of an anti-vascular endothelial growth factor monoclonal antibody for the therapy of solid tumors and other disorders. *Cancer research* **57**, 4593-4599 (1997).

33 Ferrara, N., Hillan, K. J., Gerber, H.-P. & Novotny, W. Discovery and development of bevacizumab, an anti-VEGF antibody for treating cancer. *Nature reviews Drug discovery* **3**, 391-400 (2004).

34 Ferrara, N., Hillan, K. J. & Novotny, W. Bevacizumab (Avastin), a humanized anti-VEGF monoclonal antibody for cancer therapy. *Biochemical and biophysical research communications* **333**, 328-335 (2005).

35 Li, Y.-L., Zhao, H. & Ren, X.-B. Relationship of VEGF/VEGFR with immune and cancer cells: staggering or forward? *Cancer biology & medicine* **13**, 206 (2016).

36 Daneman, R. *et al.* Wnt/β-catenin signaling is required for CNS, but not non-CNS, angiogenesis. *Proceedings of the National Academy of Sciences* **106**, 641-646 (2009).

37 Stenman, J. M. *et al.* Canonical Wnt signaling regulates organ-specific assembly and differentiation of CNS vasculature. *Science* **322**, 1247-1250 (2008).

38 Liebner, S. *et al.* Wnt/β-catenin signaling controls development of the blood–brain barrier. *Journal of Cell Biology* **183**, 409-417 (2008).

39 Zhou, Y. *et al.* Canonical WNT signaling components in vascular development and barrier formation. *The Journal of clinical investigation* **124**, 3825-3846 (2014).

40 Tran, K. A. *et al.* Endothelial β-catenin signaling is required for maintaining adult blood–brain barrier integrity and central nervous system homeostasis. *Circulation* **133**, 177-186 (2016).

41 Lengfeld, J. E. *et al.* Endothelial Wnt/beta-catenin signaling reduces immune cell infiltration in multiple sclerosis. *Proceedings of the National Academy of Sciences of the United States of America*, doi:10.1073/pnas.1609905114 (2017).

42 Hao, Y. *et al.* Integrated analysis of multimodal single-cell data. *Cell* (2021).

43 Vanlandewijck, M. *et al.* A molecular atlas of cell types and zonation in the brain vasculature. *Nature* **554**, 475-480 (2018).

44 Halpern, K. B. *et al.* Single-cell spatial reconstruction reveals global division of labour in the mammalian liver. *Nature* **542**, 352-356 (2017).

45 Munji, R. N. *et al.* Profiling the mouse brain endothelial transcriptome in health and disease models reveals a core blood-brain barrier dysfunction module. *Nat Neurosci* **22**, 1892-1902, doi:10.1038/s41593-019-0497-x (2019).

46 Jeong, H.-W. *et al.* Single-cell transcriptomics reveals functionally specialized vascular endothelium in brain. *eLife* **11**, e57520, doi:10.7554/eLife.57520 (2022).

47 Zarkada, G. *et al.* Specialized endothelial tip cells guide neuroretina vascularization and blood-retina-barrier formation. *Developmental Cell* **56**, 2237-2251. e2236 (2021).

48 Zhao, Q. *et al.* Single-cell transcriptome analyses reveal endothelial cell heterogeneity in tumors and changes following antiangiogenic treatment. *Cancer research* **78**, 2370-2382 (2018).

49 Conway, E. M., Collen, D. & Carmeliet, P. Molecular mechanisms of blood vessel growth. *Cardiovascular research* **49**, 507-521 (2001).

50 Potenta, S., Zeisberg, E. & Kalluri, R. The role of endothelial-to-mesenchymal transition in cancer progression. *British journal of cancer* **99**, 1375-1379 (2008).

51 Platel, V., Faure, S., Corre, I. & Clere, N. Endothelial-to-mesenchymal transition (EndoMT): roles in tumorigenesis, metastatic extravasation and therapy resistance. *Journal of oncology* **2019** (2019).

52 Neve, A., Cantatore, F. P., Maruotti, N., Corrado, A. & Ribatti, D. Extracellular matrix modulates angiogenesis in physiological and pathological conditions. *BioMed research international* **2014** (2014).
53 Clere, N., Renault, S. & Corre, I. Endothelial-to-mesenchymal transition in cancer. *Frontiers in Cell and Developmental Biology* **8** (2020).
54 Hogan, K. A., Ambler, C. A., Chapman, D. L. & Bautch, V. L. The neural tube patterns vessels developmentally using the VEGF signaling pathway. (2004).
55 James, J. M., Gewolb, C. & Bautch, V. L. Neurovascular development uses VEGF-A signaling to regulate blood vessel ingression into the neural tube. (2009).
56 Nguyen, H.-L. *et al.* TGF-β signaling in endothelial cells, but not neuroepithelial cells, is essential for cerebral vascular development. *Laboratory investigation* **91**, 1554-1563 (2011).
57 Goveia, J. *et al.* An integrated gene expression landscape profiling approach to identify lung tumor endothelial cell heterogeneity and angiogenic candidates. *Cancer cell* **37**, 21-36. e13 (2020).
58 Hupe, M. *et al.* Gene expression profiles of brain endothelial cells during embryonic development at bulk and single-cell levels. *Science Signaling* **10** (2017).
59 Sabbagh, M. F. *et al.* Transcriptional and epigenomic landscapes of CNS and non-CNS vascular endothelial cells. *elife* **7**, e36187 (2018).
60 del Toro, R. *et al.* Identification and functional analysis of endothelial tip cell–enriched genes. *Blood, The Journal of the American Society of Hematology* **116**, 4025-4033 (2010).
61 Coelho-Santos, V., Berthiaume, A.-A., Ornelas, S., Stuhlmann, H. & Shih, A. Y. Imaging the construction of capillary networks in the neonatal mouse brain. *Proceedings of the National Academy of Sciences* **118** (2021).
62 Uemura, A., Kusuhara, S., Katsuta, H. & Nishikawa, S.-I. Angiogenesis in the mouse retina: a model system for experimental manipulation. *Experimental cell research* **312**, 676-683 (2006).
63 Lee, H.-W. *et al.* The Role of Venous Endothelial Cells in Developmental and Pathologic Angiogenesis. *Circulation* (2021).
64 Schmidt, M. *et al.* EGFL7 regulates the collective migration of endothelial cells by restricting their spatial distribution. (2007).
65 Parker, L. H. *et al.* The endothelial-cell-derived secreted factor Egfl7 regulates vascular tube formation. *Nature* **428**, 754-758 (2004).
66 Nichol, D. *et al.* Impaired angiogenesis and altered Notch signaling in mice overexpressing endothelial Egfl7. *Blood, The Journal of the American Society of Hematology* **116**, 6133-6143 (2010).
67 Poissonnier, L., Villain, G., Soncin, F. & Mattot, V. Egfl7 is differentially expressed in arteries and veins during retinal vascular development. *PloS one* **9**, e90455 (2014).
68 Joshkon, A. *et al.* Role of CD146 (MCAM) in Physiological and Pathological Angiogenesis—Contribution of New Antibodies for Therapy. *Biomedicines* **8**, 633 (2020).
69 Jiang, T. *et al.* CD146 is a coreceptor for VEGFR-2 in tumor angiogenesis. *Blood, The Journal of the American Society of Hematology* **120**, 2330-2339 (2012).
70 Lee, K.-m. *et al.* Extracellular matrix protein 1 regulates cell proliferation and trastuzumab resistance through activation of epidermal growth factor signaling. *Breast Cancer Research* **16**, 1-17 (2014).

71 De Luca, A. *et al.* The role of the EGFR signaling in tumor microenvironment. *Journal of cellular physiology* **214**, 559-567 (2008).
72 Stoppelli, M. P. in *Madame Curie Bioscience Database [Internet]* (Landes Bioscience, 2013).
73 Takayama, Y. *et al.* Inhibition of PAI-1 limits tumor angiogenesis regardless of angiogenic stimuli in malignant pleural mesothelioma. *Cancer research* **76**, 3285-3294 (2016).
74 Zhang, G., Yang, X. & Gao, R. Research progress on the structure and function of endomucin. *Animal Models and Experimental Medicine* **3**, 325-329 (2020).
75 Park-Windhol, C. *et al.* Endomucin inhibits VEGF-induced endothelial cell migration, growth, and morphogenesis by modulating VEGFR2 signaling. *Scientific reports* **7**, 1-13 (2017).
76 Girolamo, F., Coppola, C., Ribatti, D. & Trojano, M. Angiogenesis in multiple sclerosis and experimental autoimmune encephalomyelitis. *Acta Neuropathol Commun* **2**, 84, doi:10.1186/s40478-014-0084-z (2014).
77 Kaufmann, M. *et al.* Identification of early neurodegenerative pathways in progressive multiple sclerosis. *Nat Neurosci* **25**, 944-955, doi:10.1038/s41593-022-01097-3 (2022).
78 Potente, M., Gerhardt, H. & Carmeliet, P. Basic and therapeutic aspects of angiogenesis. *Cell* **146**, 873-887, doi:10.1016/j.cell.2011.08.039 (2011).
79 Potente, M. & Carmeliet, P. The Link Between Angiogenesis and Endothelial Metabolism. *Annu Rev Physiol* **79**, 43-66, doi:10.1146/annurev-physiol-021115-105134 (2017).
80 Rohlenova, K. *et al.* Single-Cell RNA Sequencing Maps Endothelial Metabolic Plasticity in Pathological Angiogenesis. *Cell Metab* **31**, 862-877 e814, doi:10.1016/j.cmet.2020.03.009 (2020).
81 Gavalas, N. G. *et al.* VEGF directly suppresses activation of T cells from ascites secondary to ovarian cancer via VEGF receptor type 2. *British Journal of Cancer* **107**, 1869-1875, doi:10.1038/bjc.2012.468 (2012).
82 Bourhis, M., Palle, J., Galy-Fauroux, I. & Terme, M. Direct and Indirect Modulation of T Cells by VEGF-A Counteracted by Anti-Angiogenic Treatment. *Front Immunol* **12**, 616837, doi:10.3389/fimmu.2021.616837 (2021).
83 Jetten, N. *et al.* Anti-inflammatory M2, but not pro-inflammatory M1 macrophages promote angiogenesis in vivo. *Angiogenesis* **17**, 109-118 (2014).
84 Quiding-Järbrink, M., Smith, D. A. & Bancroft, G. J. Production of matrix metalloproteinases in response to mycobacterial infection. *Infection and immunity* **69**, 5661-5670, doi:10.1128/iai.69.9.5661-5670.2001 (2001).
85 Conway, D. E. & Schwartz, M. A. Mechanotransduction of shear stress occurs through changes in VE-cadherin and PECAM-1 tension: implications for cell migration. *Cell Adh Migr* **9**, 335-339, doi:10.4161/19336918.2014.968498 (2015).
86 Lengfeld, J. E. *et al.* Endothelial Wnt/β-catenin signaling reduces immune cell infiltration in multiple sclerosis. *Proceedings of the National Academy of Sciences* **114**, E1168-E1177 (2017).
87 Kim, I. *et al.* Vascular endothelial growth factor expression of intercellular adhesion molecule 1 (ICAM-1), vascular cell adhesion molecule 1 (VCAM-1), and E-selectin through nuclear factor-κB activation in endothelial cells. *Journal of Biological Chemistry* **276**, 7614-7620 (2001).

88 Argaw, A. T., Gurfein, B. T., Zhang, Y., Zameer, A. & John, G. R. VEGF-mediated disruption of endothelial CLN-5 promotes blood-brain barrier breakdown. *Proceedings of the National Academy of Sciences* **106**, 1977-1982 (2009).

89 Antonetti, D. A., Barber, A. J., Hollinger, L. A., Wolpert, E. B. & Gardner, T. W. Vascular endothelial growth factor induces rapid phosphorylation of tight junction proteins occludin and zonula occluden 1: a potential mechanism for vascular permeability in diabetic retinopathy and tumors. *Journal of Biological Chemistry* **274**, 23463-23467 (1999).

90 Murakami, T., Felinski, E. A. & Antonetti, D. A. Occludin phosphorylation and ubiquitination regulate tight junction trafficking and vascular endothelial growth factor-induced permeability. *Journal of Biological Chemistry* **284**, 21036-21046 (2009).

91 Wang, W., Dentler, W. L. & Borchardt, R. T. VEGF increases BMEC monolayer permeability by affecting occludin expression and tight junction assembly. *American Journal of Physiology-Heart and Circulatory Physiology* **280**, H434-H440 (2001).

92 Gavard, J. & Gutkind, J. S. VEGF controls endothelial-cell permeability by promoting the β-arrestin-dependent endocytosis of VE-cadherin. *Nature cell biology* **8**, 1223-1234 (2006).

93 Senger, D. R. *et al.* Tumor cells secrete a vascular permeability factor that promotes accumulation of ascites fluid. *Science* **219**, 983-985 (1983).

94 Argaw, A. T. *et al.* Astrocyte-derived VEGF-A drives blood-brain barrier disruption in CNS inflammatory disease. *J Clin Invest* **122**, 2454-2468, doi:10.1172/jci60842 (2012).

95 Vanlandewijck, M., Lebouvier, T., Mäe, M. A., Nahar, K. & Betsholtz, C. Primary isolation of vascular cells from murine brain for single cell sequencing. (2018).

96 Yuan, J. & Sims, P. A. An Automated Microwell Platform for Large-Scale Single Cell RNA-Seq. *Sci Rep* **6**, 33883, doi:10.1038/srep33883 (2016).

97 Yuan, J. *et al.* Single-cell transcriptome analysis of lineage diversity in high-grade glioma. *Genome Med* **10**, 57, doi:10.1186/s13073-018-0567-9 (2018).

98 Menon, V. Clustering single cells: a review of approaches on high-and low-depth single-cell RNA-seq data. *Brief Funct Genomics* **17**, 240-245, doi:10.1093/bfgp/elx044 (2018).

99 Cembrowski, M. S. & Menon, V. Continuous Variation within Cell Types of the Nervous System. *Trends Neurosci* **41**, 337-348, doi:10.1016/j.tins.2018.02.010 (2018).

100 Tasic, B. *et al.* Adult mouse cortical cell taxonomy revealed by single cell transcriptomics. *Nat Neurosci* **19**, 335-346, doi:10.1038/nn.4216 (2016).

101 Sorensen, S. A. *et al.* Correlated gene expression and target specificity demonstrate excitatory projection neuron diversity. *Cereb Cortex* **25**, 433-449, doi:10.1093/cercor/bht243 (2015).

102 Hawrylycz, M. *et al.* Canonical genetic signatures of the adult human brain. *Nat Neurosci* **18**, 1832-1844, doi:10.1038/nn.4171 (2015).

103 Mazzoni, J. *et al.* The Wnt Inhibitor Apcdd1 Coordinates Vascular Remodeling and Barrier Maturation of Retinal Blood Vessels. *Neuron* **96**, 1055-1069 e1056, doi:10.1016/j.neuron.2017.10.025 (2017).

FIGURE LEGENDS

Figure 1. Single-cell RNA sequencing and analysis of spinal cord endothelial cells from control and MOG_{35-55} EAE mice reveals clustering driven by zonation followed by disease/healthy state. a) Schematic diagram of the experimental workflow for the isolation and transcriptomic profiling of endothelial cells (ECs) from either healthy (orange), CFA (yellow), acute (blue) or chronic (magenta) MOG_{35-55} experimental autoimmune encephalomyelitis (EAE). **b**) Architecture of the mammalian vascular system depicting arteries, capillaries, venules and veins and some of their specific molecular markers. **c**) t-SNE visualization of the 23 distinct EC clusters within the scRNAseq dataset. **d**) t-SNE plot color-coded by sample condition. ECs from acute (blue) and chronic (magenta) EAE samples cluster separately from control ECs [healthy (orange) and CFA (yellow)], suggestive of transcriptional shifts in ECs from both acute and chronic EAE. **e**) Feature plots show the distribution of arterial (*Bmx*), capillary (*Slc1a1*), and venous (*Nr2f2*) marker expression within the t-SNE plot. Expression of arterial and venous markers peaks at the opposite ends of the t-SNE plot separated by the capillary marker expression in the middle indicative that zonation is an important axis of variation among the cells. **f**) Dot plot illustrating the expression of several arterial-, capillary-, and venous-specific markers within the 23 EC clusters in the scRNAseq dataset. Clusters are annotated based on marker gene expression.

Figure 2. Endothelial subtype-specific t-SNE plots for spinal cords ECs isolated from control and EAE mice show separation of capillary and venous ECs in acute and chronic EAE from the healthy/CFA state. a, d, g, j) Individual t-SNE plots for arterial (aECs; a), capillary (cECs; d), venule (vnECs; g) and vein ECs (vECs; j) color-coded for sample type. **b, e, h, k**) Individual t-SNE plots for aECs (b), cECs (e), vnECs (h) and vECs (k), respectively, depict the clustering of

healthy (orange), disease control (CFA; yellow), acute (blue) and chronic (purple) EAE ECs for each vessel subtype. There is no clear separation in either the clustering or the t-SNE visualization between controls and chronic EAE (gray) in aECs and controls (healthy vs. CFA; gray) in vnECs and vECs. **c, f, i, l**) Stacked plots showing the percentage of ECs from each sample type (healthy, CFA, acute or chronic EAE) within the aECs (c), cECs (f), vnECs (i) and vECs (l) t-SNE plots, respectively.

Figure 3. Gene set enrichment analysis (GSEA) reveals that transcriptome signatures of neo-angiogenesis are present in vein ECs from both acute and chronic EAE. a, c) Pathways/processes upregulated in diseased arterial (red), capillary (light gray), venule (dark blue), and venous (light blue) ECs in acute (a; 16 d.p.i) and chronic (c, 28 d.p.i) EAE versus controls. The gene ontology enrichment plots, derived using the GSEA algorithm, indicate that gene sets related to neo-angiogenesis (highlighted in red) are significantly upregulated in diseased vECs, and to a lesser extent, vnECs, relative to controls, in both acute and chronic EAE. **b, d**) Pathways/processes significantly downregulated in diseased arterial (red), capillary (gray), venule (venetian blue) and venous (pool blue) ECs in acute (b), and chronic (d), EAE versus controls. Expression of the blood-brain barrier gene set is significantly reduced in diseased ECs of all vessel subtypes, except arteries. **e**) Dot plots for expression of angiogenesis, tip cells, EC migration, extracellular matrix, VEGF and TGF-β pathway genes in vECs show increased average expression in both acute and chronic EAE. vnECs also upregulate expression of tip cell markers in acute and chronic EAE.

Figure 4. Vein EC show increased proliferation in both acute and chronic EAE. a) Schematic diagram of the spinal cord longitudinal (sagittal) sections used throughout the study to measure *in vivo* protein/mRNA expression in blood vessels of either control or EAE mice. **b**) Dot plot shows that *Mki67* mRNA expression is increased in acute, and to a lesser extent chronic, EAE vECs by scRNAseq. **c, c', c'', c'''**) Analysis of Ki67 expression in Vcam1$^+$ endothelium shows increased vEC proliferation in acute and chronic EAE, relative to control (CFA). **d, d', d'', d'''**) Analysis of Ki67 expression in Mfsd2a$^+$ ECs reveal that capillary ECs do not proliferate during neuroinflammation. **e, e', e'', e'''**) Analysis of Ki67 expression in αSMA surrounded CD31$^+$ aEC reveal that arterial ECs do not proliferate in acute or chronic EAE. **f**) Dotted bar graph shows the percentage of Ki67$^+$ Vcam1$^+$ vECs in control, acute and chronic EAE. There is a significant upregulation of vEC proliferation in EAE, relative to controls. **g**) Dotted bar graph shows the percentage of vein coverage in CFA control, acute and chronic EAE spinal cords. Vein density is increased significantly in both acute and chronic EAE. Graphs represent mean ± SEM from n = 5 mice/group; *$p < 0.05$, **$p < 0.01$, ****$p < 0.0001$; one-way ANOVA with Bonferroni's multiple comparisons test. Scale bars = 100 μm.

Figure 5. Expression of several angiogenic markers is upregulated by ECs at acute EAE. a, d, g, j, m) Violin plots for *Egfl7*, *Mcam*, *Ecm1*, *Serpine1* and *Emcn* mRNA expression in control (healthy and CFA), acute and chronic EAE vECs generated from the scRNAseq data. **b-b'', h-h'', k-k''**) Fluorescence in situ hybridization (FISH) for *Egfl7*, *Ecm1* and *Serpine1* mRNAs (red) combined with immunofluorescence for Caveolin-1 (green; EC marker) in CFA (control), acute and chronic EAE in inflamed white matter vessels (DAPI not shown). **e-e'', n-n''**) Immunofluorescence for Mcam, Emcn and Caveolin-1 in CFA (control), acute and chronic

MOG_{35-55} EAE spinal cords in inflamed white matter vessels (DAPI not shown). **c, f, i, l, o**) Dotted bar graphs show the relative expression levels of *Egfl7*, Mcam, *Ecm1*, *Serpine1* and Emcn in acute and chronic EAE, compared to control (CFA), spinal cord blood vessels. Data represent mean ± SEM; *p < 0.05, **p < 0.01, ****p < 0.0001; one-way ANOVA with Bonferroni's multiple comparisons test. Scale bars = 100 μm.

Figure 6. Increased vessel density and expression of angiogenic markers in human multiple sclerosis lesions. a, a', a'') Immunohistochemistry (IHC) staining for CD31 (EC marker) in white matter (WM) lesions of MS patients (a), normal appearing white matter (NAWM) of an MS patient (a') or a non-neurological control case (a''). The average $CD31^+$ vessel density per area is increased in the MS lesion compared to NAWM from MS patient or non-neurological controls. **b, b', b''**) IHC for the angiogenic marker, EGFL7, shows increased expression in WM lesions of MS patients (b) relative to NAWM of both the MS (b') and a non-neurological control case (b''). **c, c', c''**) IHC for the angiogenic marker, MCAM, shows increased expression in both the WM lesions and NAWM of MS cases (c and c', respectively), relative to NAWM of non-neurological control case (c''). **b-c''**) Hematoxylin was used as a nuclear counterstain. **d, e, f**) Dotted bar graphs of the $CD31^+$ average vessel density per given area (d), average EGFL7 (e), and MCAM (f) expression in blood vessels located in WM lesions and NAWM of MS patients (N = 6) and NAWM of non-neurological control patients (N=6). Data represent mean ± SEM; *p < 0.05, **p < 0.01, ****p < 0.0001; two-tailed Student's t test. Scale bars = 200 μm.

Figure 7. Gene set enrichment analysis (GSEA) reveals that transcriptome signatures of neo-angiogenesis are downregulated in spinal cord ECs of acute EAE mice following treatment

with bevacizumab. a) Diagram of the experimental procedure. Following EAE induction, mice were injected intraperitoneally (i. p.) every 7 days with either 5 mg/kg anti-VEGF monoclonal antibody bevacizumab, or an isotype control immunoglobulin G1 (IgG1), from 7 d.p.i until 40 d.p.i. (chronic phase). **b**) Clinical EAE score curves for all, and surviving, bevacizumab-, and IgG1-treated, mice. The inset pie charts depict the fraction of mice with no EAE (blue), mice that developed clinical EAE (pink), or mice that died from EAE (yellow), in the two treatment groups. The IgG1-treated EAE mice exhibit significantly higher incidence of death (clinical score = 6) compared to the bevacizumab-treated EAE mice. **c, d, e**) Dotted bar graphs of the day of disease onset (c), peak clinical score (d), and score on the day of collection (e), for the two EAE groups. No significant difference was found in the day of disease onset between bevacizumab- and IgG1-treated EAE mice. Peak clinical score and clinical score on the day of collection (40 d.p.i) were significantly lower for bevacizumab- compared to IgG1-treated EAE mice. **f**) t-SNE visualization of ECs isolated from either CFA, acute EAE and BevAc EAE spinal cords, color-coded for the sample type. **g**) t-SNE plot, color-coded for EC subtype, shows that BevAc ECs in this representation are visually organized along the arteriovenous zonation gradient. **h**) Pathways/processes significantly downregulated in BevAc EAE ECs relative to untreated acute EAE ECs. The gene ontology enrichment plots, derived using the GSEA algorithm, shows that expression of neo-angiogenic gene sets and pathways (highlighted in red) is significantly downregulated in BevAc EAE ECs, relative to untreated acute EAE ECs. **i**) Dot plots of the expression of some blood-brain barrier genes regulating cell junctions and caveolae in BevAc ECs, compared to either CFA, or acute EAE ECs. Data represent mean ± SEM; * $p < 0.05$, ** $p < 0.01$, **** $p < 0.0001$; b) one-way ANOVA with repeated measures; c, d, e) two-tailed Student's t-test.

Figure 8. Bevacizumab treatment reduces expression of neo-angiogenesis markers by vein ECs in EAE. a-e) Violin plots depicting changes in *Egfl7*, *Mcam*, *Ecm1*, *Serpine1* and *Emcn* expression levels in BevCh ECs (acute EAE) relative to CFA control and untreated acute EAE ECs (16 d.p.i.). **f-j'**) Fluorescence in situ hybridization for *Egfl7* (f, f'), *Ecm1* (h, h') and *Serpine1* (I, i') mRNAs, and immunofluorescence for Mcam (g, g') and Emcn (j, j') proteins, combined with Caveolin-1 (EC marker), in spinal cord blood vessels from IgG1- and bevacizumab-treated EAE mice in chronic disease (40 d.p.i). *Egfl7*, *Ecm1*, *Serpine1* and Emcn are highly expressed in blood vessels of IgG-treated, but not bevacizumab-treated, chronic EAE mice. Vascular Mcam expression is absent in spinal cord tissue in chronic EAE. **k-n**) Dotted bar graphs show relative vascular levels for either *Egfl7*, *Ecm1*, *Serpine1* mRNAs, or Emcn and Mcam proteins, in bevacizumab- and IgG1-treated chronic EAE mice. Expression of all angiogenesis markers, except Mcam, is significantly reduced in bevacizumab-treated chronic EAE mice, relative to IgG controls. **p**) Vein coverage ($Vcam1^+$ area) is slightly reduced ($p = 0.0742$) in the spinal cord blood vessels of bevacizumab- relative to IgG1-treated (control) chronic EAE mice. Data represent mean ± SEM from n = 6 mice/group; * $p<0.05$, ** $p<0.01$; **** $p<0.0001$; unpaired two-sided Student's t-test. **q**) Model illustrating the putative mechanism of pathological neo-angiogenesis in EAE. Neuroinflammation induces formation of leaky, dysfunctional, new blood vessels via neo-angiogenesis from inflamed veins located in the white matter lesions of the spinal cord, where there is a significant presence of infiltrating immune cells. Hypoxic conditions within the inflamed CNS induce secretion of VEGF-A (green) from either infiltrating immune cells (e.g. macrophages), or CNS resident cells (e.g. astrocytes), resulting in activation of VEGF-A signaling pathway in vECs. Blockade of VEGF signaling through administration of bevacizumab reduces

1131 neo-angiogenesis and disease severity, demonstrating that VEGF-A signaling is a key driver of

1132 neo-angiogenesis in neuroinflammation.

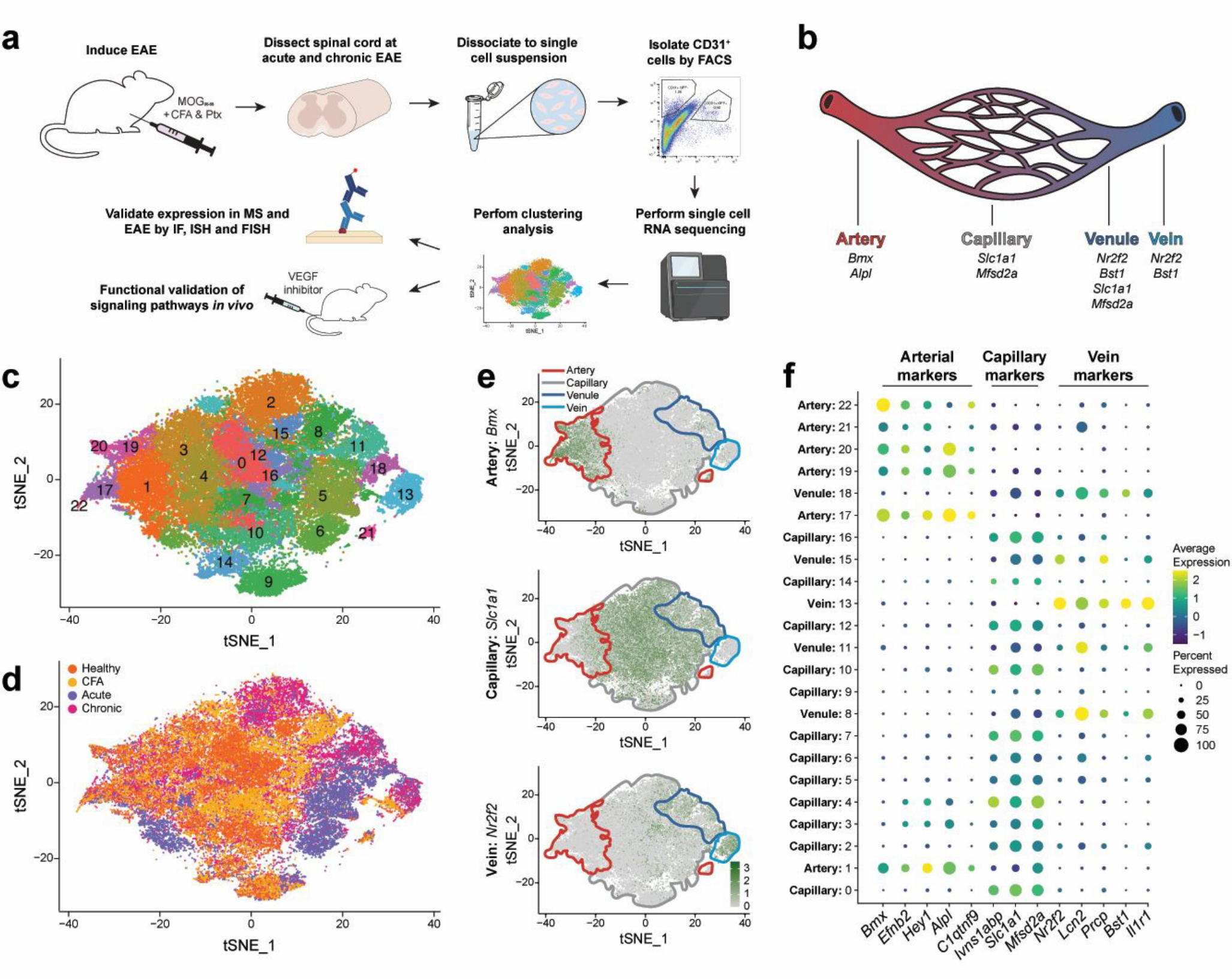
a
Induce EAE
MOG
+CFA & Ptx
Dissect spinal cord at acute and chronic EAE
Dissociate to single cell suspension
Isolate CD31+ cells by FACS
Perform single cell RNA sequencing
Perfom clustering analysis
Validate expression in MS and EAE by IF, ISH and FISH
Functional validation of signaling pathways in vivo
VEGF inhibitor
b
Artery
Bmx
Alpl
Capillary
Slc1a1
Mfsd2a
Venule
Nr2f2
Bst1
Slc1a1
Mfsd2a
Vein
Nr2f2
Bst1
c
tSNE_1
tSNE_2
d
Healthy
CFA
Acute
Chronic
e
Artery
Capillary
Venule
Vein
Artery: Bmx
Capillary: Slc1a1
Vein: Nr2f2
f
Arterial markers
Capillary markers
Vein markers
Artery: 22
Artery: 21
Artery: 20
Artery: 19
Venule: 18
Artery: 17
Capillary: 16
Venule: 15
Capillary: 14
Vein: 13
Capillary: 12
Venule: 11
Capillary: 10
Capillary: 9
Venule: 8
Capillary: 7
Capillary: 6
Capillary: 5
Capillary: 4
Capillary: 3
Capillary: 2
Artery: 1
Capillary: 0
Bmx
Efnb2
Hey1
Alpl
C1qtnf9
Ivns1abp
Slc1a1
Mfsd2a
Nr2f2
Lcn2
Prcp
Bst1
Il1r1
Average Expression
Percent Expressed

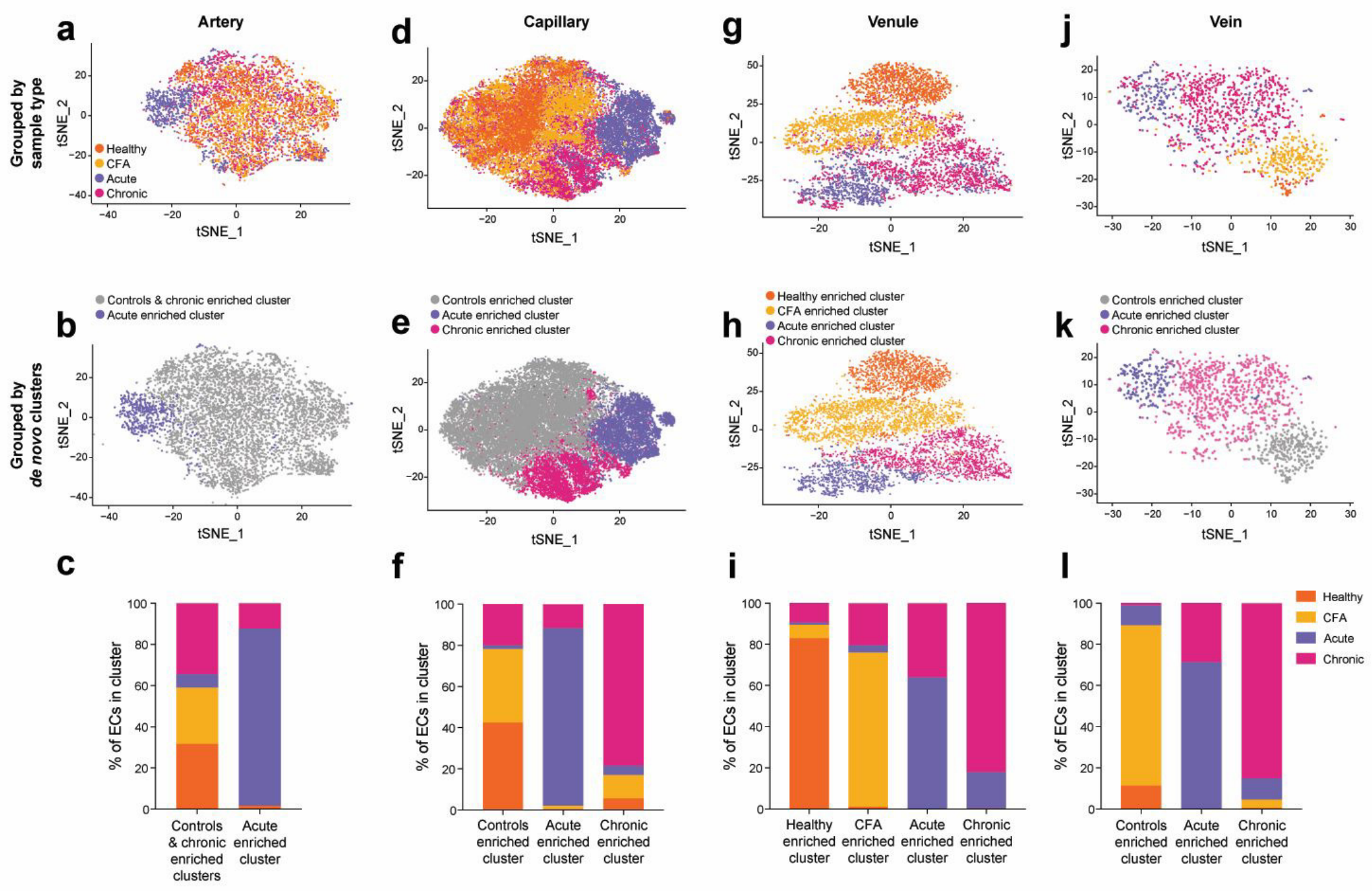
a
Artery
Grouped by sample type
Healthy
CFA
Acute
Chronic
tSNE_1
tSNE_2
d
Capillary
g
Venule
j
Vein
b
Controls & chronic enriched cluster
Acute enriched cluster
Grouped by de novo clusters
e
Controls enriched cluster
Acute enriched cluster
Chronic enriched cluster
h
Healthy enriched cluster
CFA enriched cluster
Acute enriched cluster
Chronic enriched cluster
k
Controls enriched cluster
Acute enriched cluster
Chronic enriched cluster
c
% of ECs in cluster
Controls & chronic enriched clusters
Acute enriched cluster
f
Controls enriched cluster
Acute enriched cluster
Chronic enriched cluster
i
Healthy enriched cluster
CFA enriched cluster
Acute enriched cluster
Chronic enriched cluster
l
Healthy
CFA
Acute
Chronic
Controls enriched cluster
Acute enriched cluster
Chronic enriched cluster

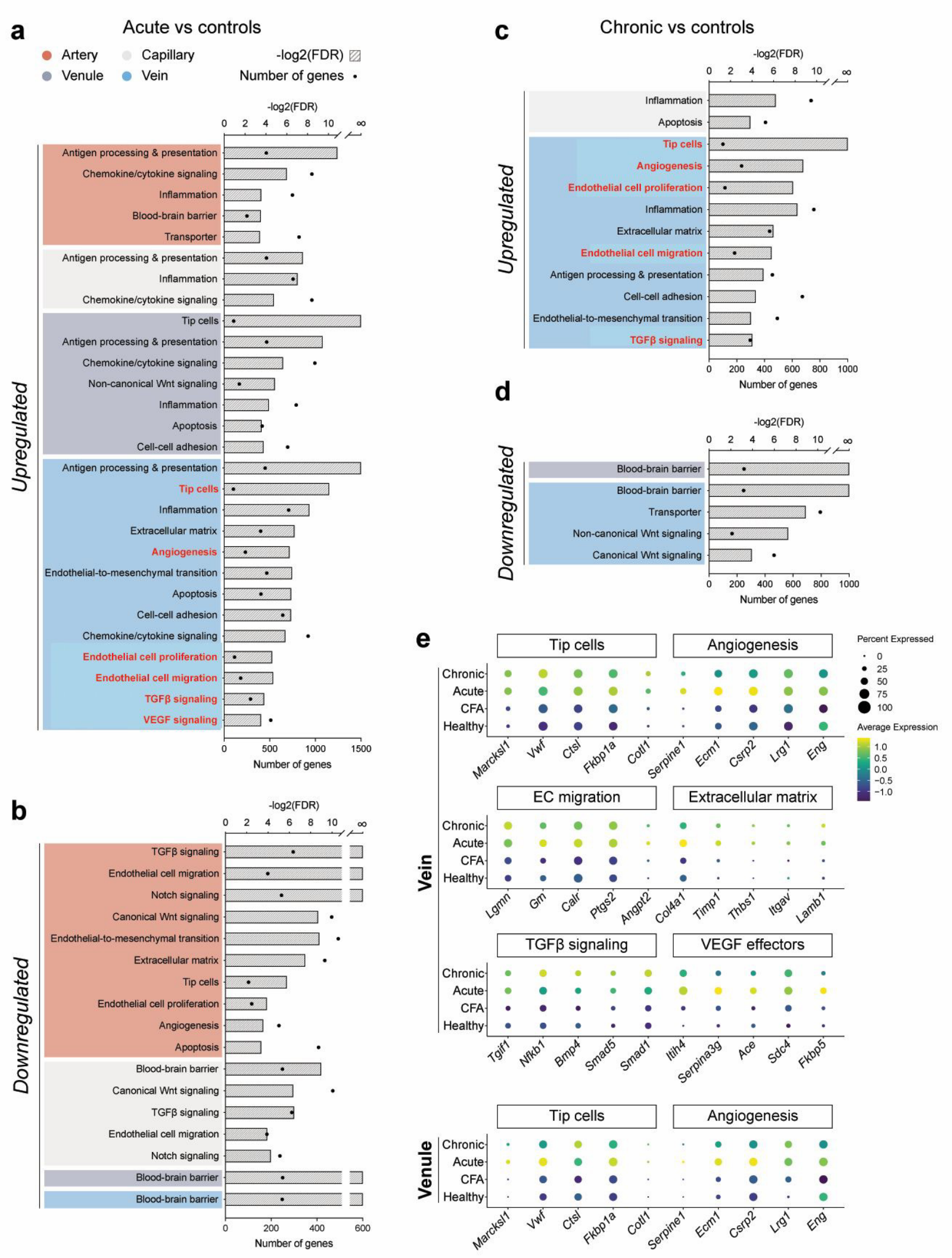
a
Acute vs controls
Artery
Capillary
Venule
Vein
-log2(FDR)
Number of genes
Upregulated
Antigen processing & presentation
Chemokine/cytokine signaling
Inflammation
Blood-brain barrier
Transporter
Antigen processing & presentation
Inflammation
Chemokine/cytokine signaling
Tip cells
Antigen processing & presentation
Chemokine/cytokine signaling
Non-canonical Wnt signaling
Inflammation
Apoptosis
Cell-cell adhesion
Antigen processing & presentation
Tip cells
Inflammation
Extracellular matrix
Angiogenesis
Endothelial-to-mesenchymal transition
Apoptosis
Cell-cell adhesion
Chemokine/cytokine signaling
Endothelial cell proliferation
Endothelial cell migration
TGFβ signaling
VEGF signaling
b
Downregulated
TGFβ signaling
Endothelial cell migration
Notch signaling
Canonical Wnt signaling
Endothelial-to-mesenchymal transition
Extracellular matrix
Tip cells
Endothelial cell proliferation
Angiogenesis
Apoptosis
Blood-brain barrier
Canonical Wnt signaling
TGFβ signaling
Endothelial cell migration
Notch signaling
Blood-brain barrier
Blood-brain barrier
c
Chronic vs controls
Upregulated
Inflammation
Apoptosis
Tip cells
Angiogenesis
Endothelial cell proliferation
Inflammation
Extracellular matrix
Endothelial cell migration
Antigen processing & presentation
Cell-cell adhesion
Endothelial-to-mesenchymal transition
TGFβ signaling
d
Downregulated
Blood-brain barrier
Blood-brain barrier
Transporter
Non-canonical Wnt signaling
Canonical Wnt signaling
e
Vein
Venule
Tip cells
Angiogenesis
EC migration
Extracellular matrix
TGFβ signaling
VEGF effectors
Chronic
Acute
CFA
Healthy
Marcksl1
Vwf
Ctsl
Fkbp1a
Cotl1
Serpine1
Ecm1
Csrp2
Lrg1
Eng
Lgmn
Gm
Calr
Ptgs2
Angpt2
Col4a1
Timp1
Thbs1
Itgav
Lamb1
Tgif1
Nfkb1
Bmp4
Smad5
Smad1
Itih4
Serpina3g
Ace
Sdc4
Fkbp5
Percent Expressed
Average Expression

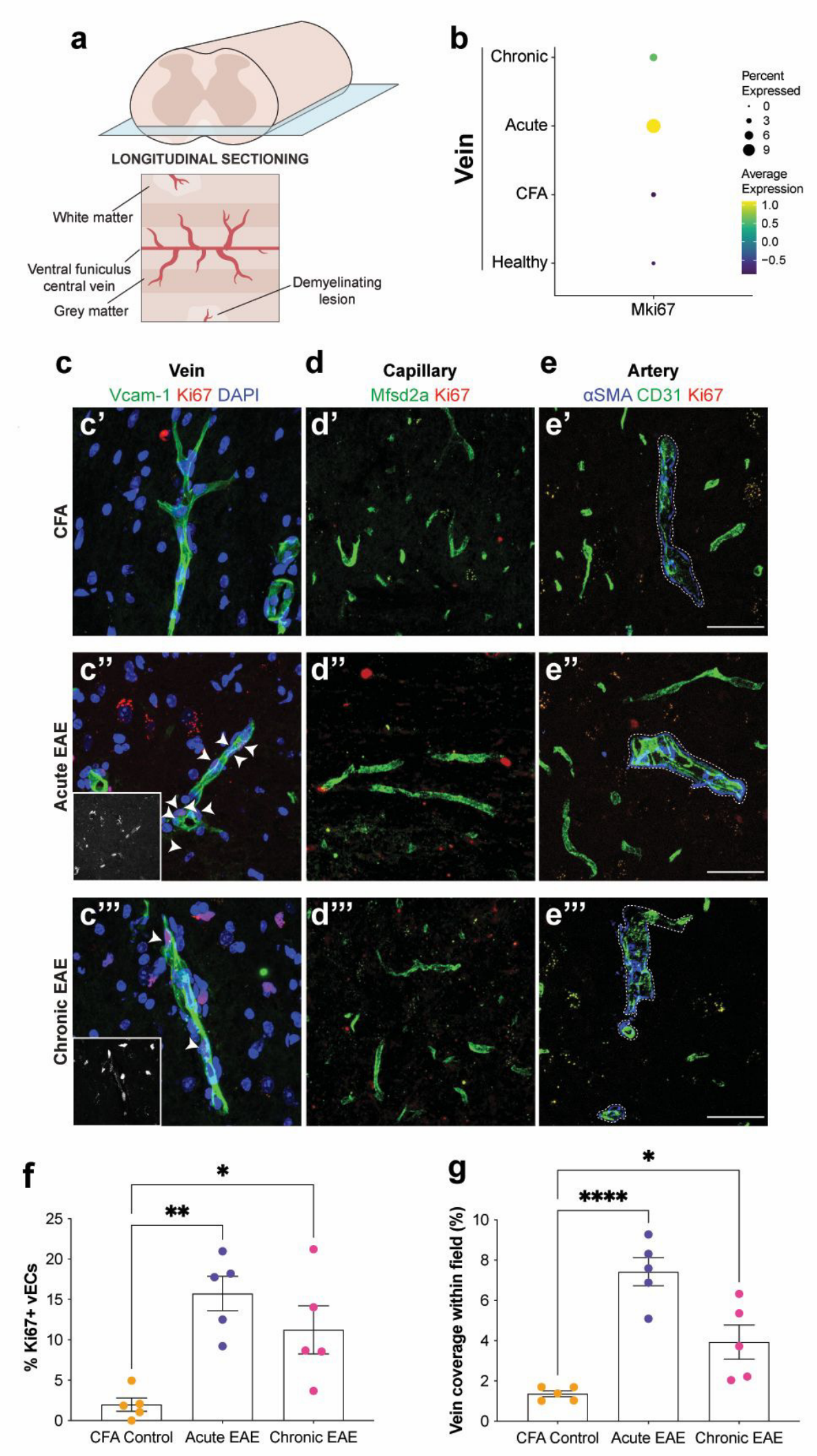
a
LONGITUDINAL SECTIONING
White matter
Ventral funiculus
central vein
Grey matter
Demyelinating
lesion
b
Vein
Chronic
Acute
CFA
Healthy
Mki67
Percent
Expressed
0
3
6
9
Average
Expression
1.0
0.5
0.0
−0.5
c
Vein
Vcam-1 Ki67 DAPI
d
Capillary
Mfsd2a Ki67
e
Artery
αSMA CD31 Ki67
c'
d'
e'
CFA
c''
d''
e''
Acute EAE
c'''
d'''
e'''
Chronic EAE
f
% Ki67+ vECs
25
20
15
10
5
0
**
*
CFA Control
Acute EAE
Chronic EAE
g
Vein coverage within field (%)
10
8
6
4
2
0
****
*
CFA Control
Acute EAE
Chronic EAE

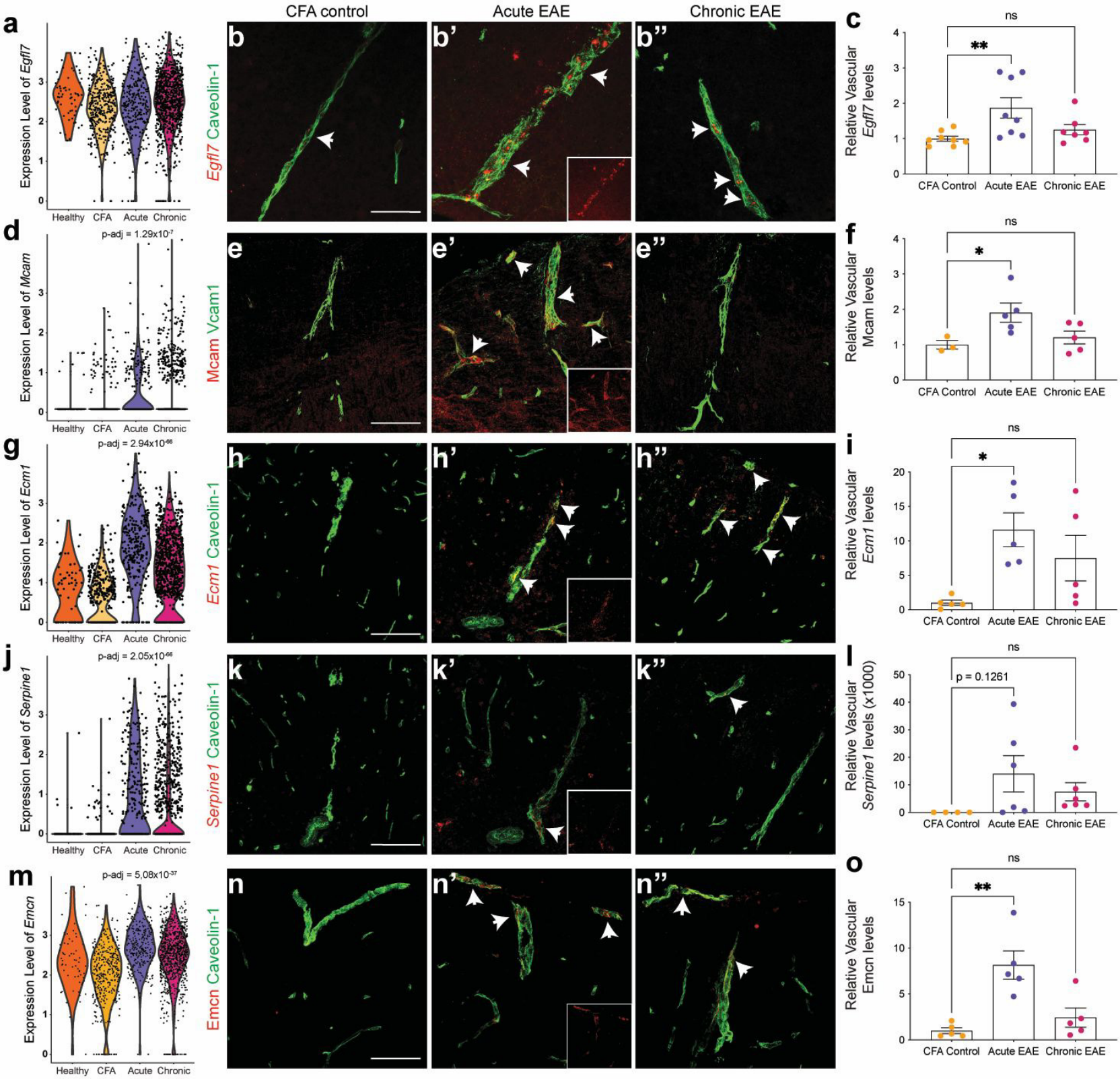
CFA control
Acute EAE
Chronic EAE
a
Expression Level of Egfl7
Healthy
CFA
Acute
Chronic
b
b'
b''
Egfl7 Caveolin-1
c
ns
**
Relative Vascular Egfl7 levels
CFA Control
Acute EAE
Chronic EAE
d
p-adj = 1.29x10-7
Expression Level of Mcam
e
e'
e''
Mcam Vcam1
f
ns
*
Relative Vascular Mcam levels
g
p-adj = 2.94x10-66
Expression Level of Ecm1
h
h'
h''
Ecm1 Caveolin-1
i
ns
*
Relative Vascular Ecm1 levels
j
p-adj = 2.05x10-66
Expression Level of Serpine1
k
k'
k''
Serpine1 Caveolin-1
l
ns
p = 0.1261
Relative Vascular Serpine1 levels (x1000)
m
p-adj = 5,08x10-37
Expression Level of Emcn
n
n'
n''
Emcn Caveolin-1
o
ns
**
Relative Vascular Emcn levels

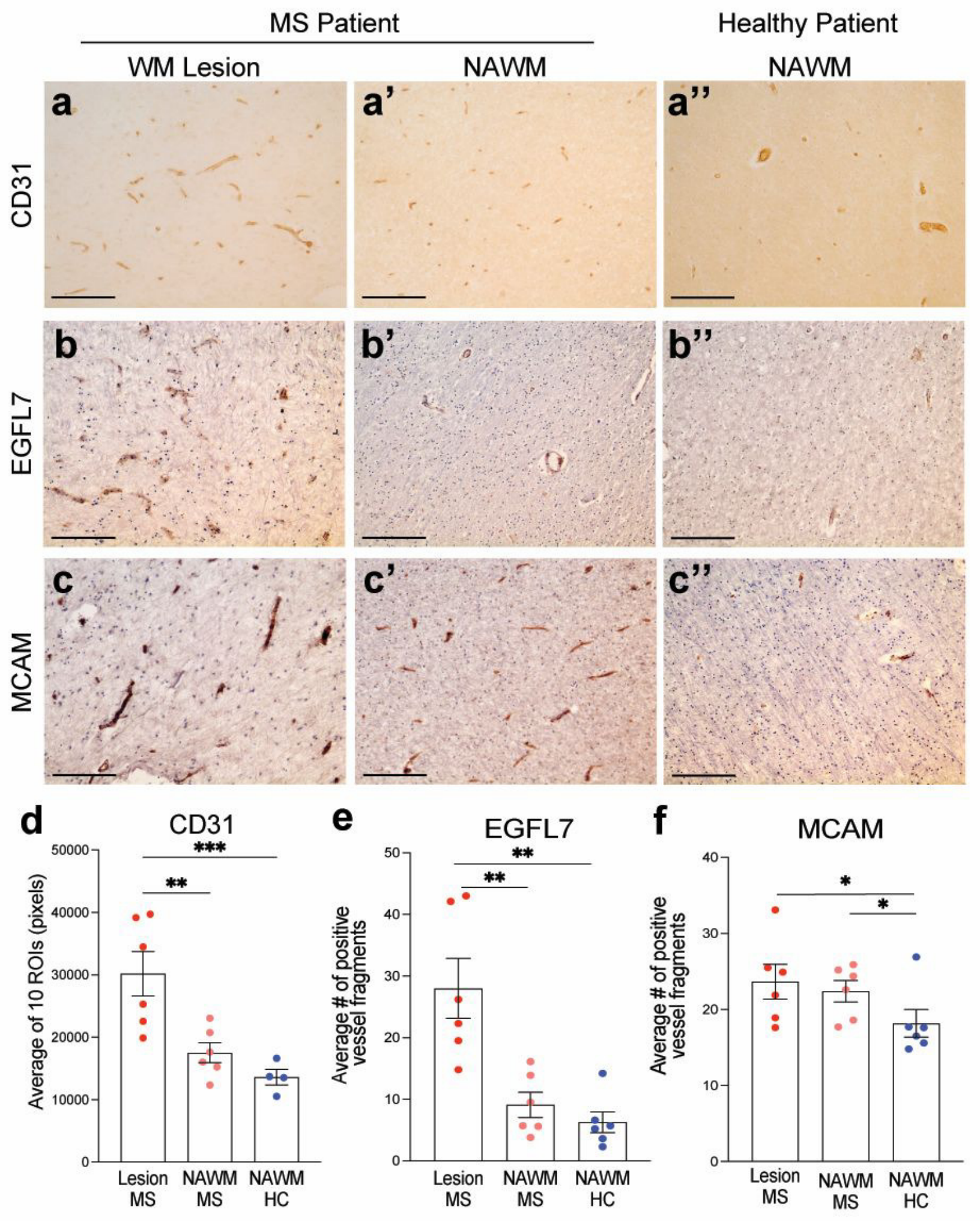
MS Patient
Healthy Patient
WM Lesion
NAWM
NAWM
a
a'
a''
CD31
b
b'
b''
EGFL7
c
c'
c''
MCAM
d
CD31
Average of 10 ROIs (pixels)
50000
40000
30000
20000
10000
0
***
**
Lesion MS
NAWM MS
NAWM HC
e
EGFL7
Average # of positive vessel fragments
50
40
30
20
10
0
**
**
Lesion MS
NAWM MS
NAWM HC
f
MCAM
Average # of positive vessel fragments
40
30
20
10
0
*
*
Lesion MS
NAWM MS
NAWM HC

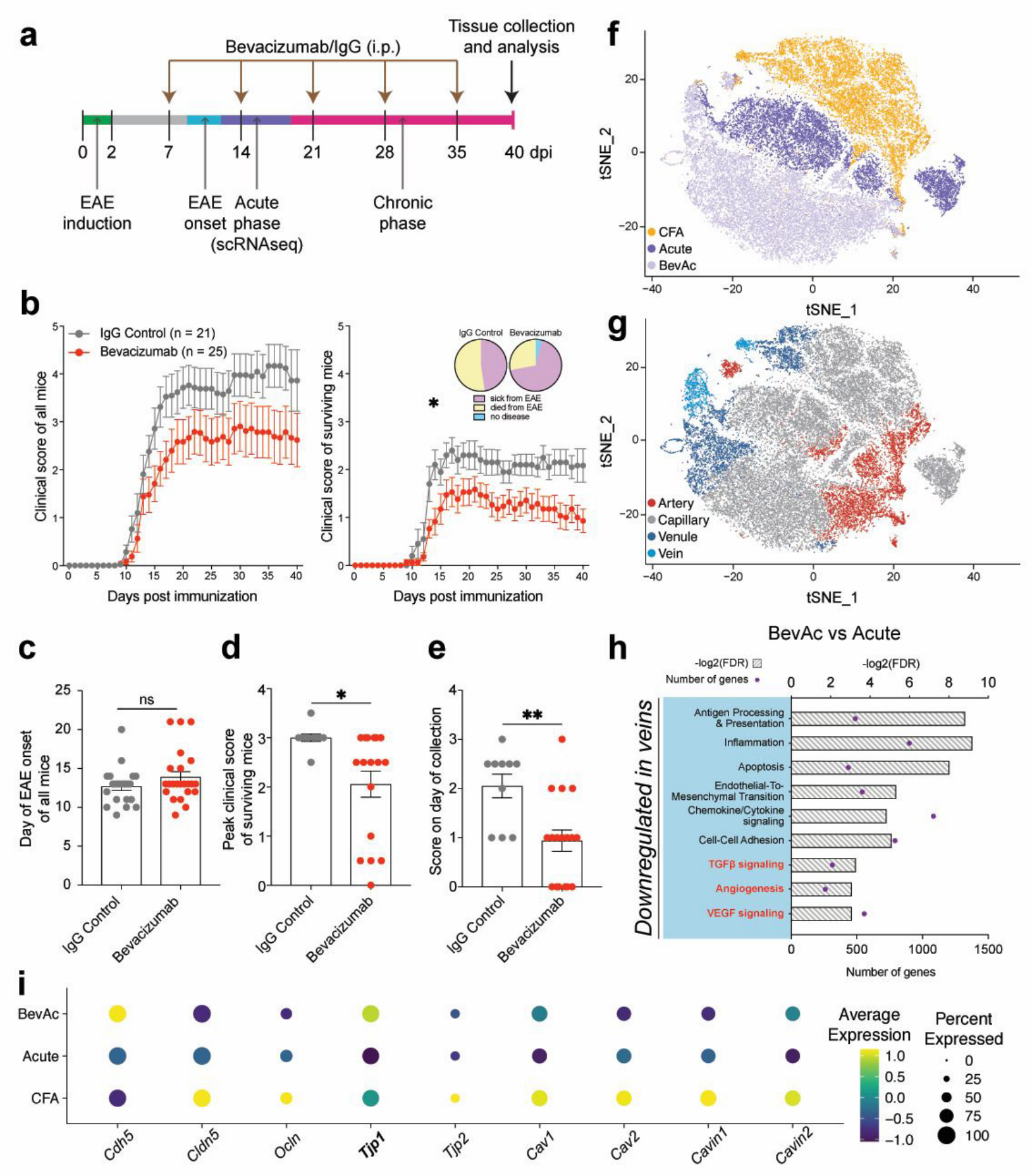
a
Bevacizumab/IgG (i.p.)
Tissue collection and analysis
0 2 7 14 21 28 35 40 dpi
EAE induction
EAE onset
Acute phase (scRNAseq)
Chronic phase
b
IgG Control (n = 21)
Bevacizumab (n = 25)
Clinical score of all mice
Days post immunization
Clinical score of surviving mice
IgG Control
Bevacizumab
sick from EAE
died from EAE
no disease
c
Day of EAE onset of all mice
ns
IgG Control
Bevacizumab
d
Peak clinical score of surviving mice
*
e
Score on day of collection
**
f
tSNE_1
tSNE_2
CFA
Acute
BevAc
g
Artery
Capillary
Venule
Vein
h
BevAc vs Acute
-log2(FDR)
Number of genes
Downregulated in veins
Antigen Processing & Presentation
Inflammation
Apoptosis
Endothelial-To-Mesenchymal Transition
Chemokine/Cytokine signaling
Cell-Cell Adhesion
TGFβ signaling
Angiogenesis
VEGF signaling
i
BevAc
Acute
CFA
Cdh5
Cldn5
Ocln
Tjp1
Tjp2
Cav1
Cav2
Cavin1
Cavin2
Average Expression
Percent Expressed

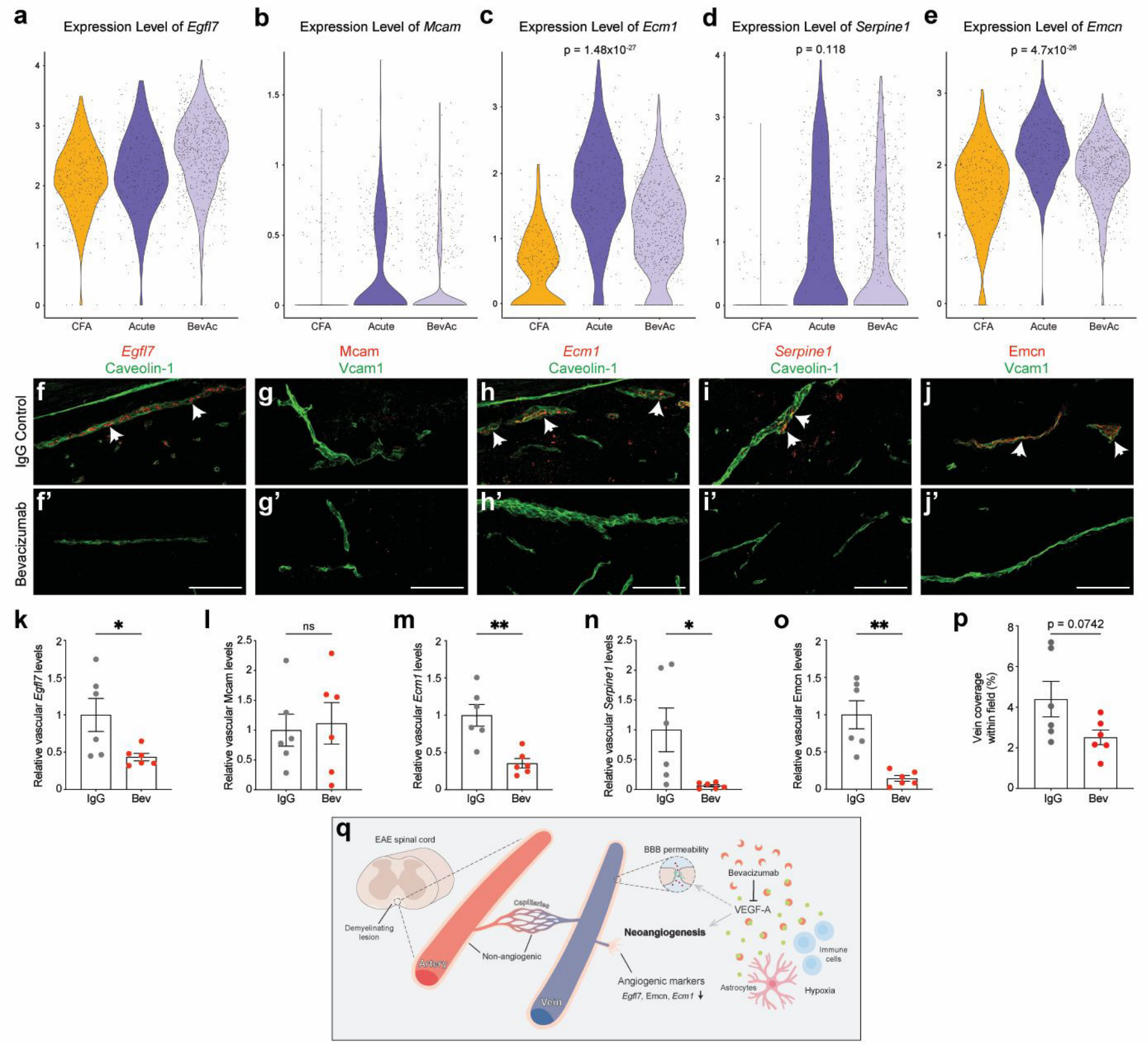
a
Expression Level of Egfl7
b
Expression Level of Mcam
c
Expression Level of Ecm1
p = 1.48x10-27
d
Expression Level of Serpine1
p = 0.118
e
Expression Level of Emcn
p = 4.7x10-26
CFA
Acute
BevAc
Egfl7
Caveolin-1
Mcam
Vcam1
Ecm1
Caveolin-1
Serpine1
Caveolin-1
Emcn
Vcam1
IgG Control
Bevacizumab
f
g
h
i
j
f'
g'
h'
i'
j'
k
Relative vascular Egfl7 levels
*
l
Relative vascular Mcam levels
ns
m
Relative vascular Ecm1 levels
**
n
Relative vascular Serpine1 levels
*
o
Relative vascular Emcn levels
**
p
Vein coverage within field (%)
p = 0.0742
IgG
Bev
q
EAE spinal cord
Demyelinating lesion
Capillaries
Non-angiogenic
Artery
Vein
BBB permeability
Bevacizumab
VEGF-A
Neoangiogenesis
Angiogenic markers
Egfl7, Emcn, Ecm1 ↓
Immune cells
Astrocytes
Hypoxia